Cretaceous exhumation of the Triassic intracontinental Xuefengshan Belt: Delayed unroofing of an orogenic plateau across the South China Block?

Yang Chu, Wei Lin, Michel Faure, Mark Allen, Zhentian Feng

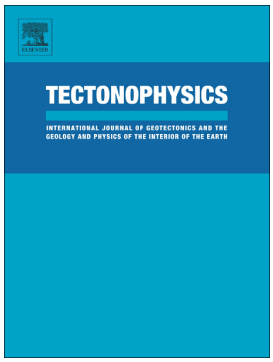

Cretaceous exhumation of the Triassic intracontinental Xuefengshan Belt: Delayed unroofing of an orogenic plateau across the South China Block?

Yang Chu, Wei Lin, Michel Faure, Mark B. Allen, Zhentian Feng

PII: S0040-1951(20)30275-4

DOI: https://doi.org/10.1016/j.tecto.2020.228592

Reference: TECTO 228592

To appear in: *Tectonophysics*

Received date: 22 May 2020

Revised date: 8 August 2020

Accepted date: 11 August 2020

Please cite this article as: Y. Chu, W. Lin, M. Faure, et al., Cretaceous exhumation of the Triassic intracontinental Xuefengshan Belt: Delayed unroofing of an orogenic plateau across the South China Block?, *Tectonophysics* (2020), https://doi.org/10.1016/j.tecto.2020.228592

Cretaceous exhumation of the Triassic intracontinental Xuefengshan Belt: delayed unroofing of an orogenic plateau across the South China Block?

Yang Chu[1,2,3,*], Wei Lin[1,2], Michel Faure[4], Mark B. Allen[3], Zhentian Feng[1,2]

1. State Key Laboratory of Lithospheric Evolution, Institute of Geology and Geophysics, Institutions of Earth Sciences, Chinese Academy of Sciences, Beijing 100029, China

2. University of Chinese Academy of Sciences, Beijing 100049, China

3. Department of Earth Sciences, University of Durham, Durham DH1 3LE, UK

4. Institut des Sciences de la Terre d'Orléans, UMR 7327, Université d'Orléans, Orléans 45071, France.

*Corresponding author. Yang Chu (chuyang@mail.iggcas.ac.cn), Institute of Geology and Geophysics, Chinese Academy of Sciences, 19 Beitucheng western Road, Chaoyang District, 100029 Beijing, P. R. China

Abstract:

A large plateau can be produced by crustal thickening in convergent zones such as continental collision belts and Andean-type subduction zones, but the life cycles of such plateaux are not well-understood. In particular, it is not clear how long they persist after construction, before other tectonic processes or erosion reduce crustal thickness and elevation to near-normal levels. Triassic subduction- and collision-tectonics produced intense deformation, magmatism and metamorphism across the entire South China Block. This large-scale crustal shortening created a broad orogenic belt, uplifted most parts of the South China Block, and probably initiated the growth of an orogenic plateau. Our study presents low-temperature thermochronology data from the Xuefengshan Belt in the interior of the South China Block. There was along-strike variation in exhumation. The north orogenic core was subjected to Triassic (~245-210 Ma), and Late Cretaceous (~100-80 Ma) exhumation, whereas the cooling path of the south orogenic core reflects a two stage Cretaceous evolution. The variable exhumation pattern reflects non-uniform tectonics in different regions, but both regions were subject to Late Cretaceous extension. We tentatively reconstruct the original plateau paleo-elevation to be ~1.5 km above sea level, based on the amount of exhumation (~10 km) and the present crustal thickness (~35 km). The T-t trajectories of the Xuefengshan Belt and other Triassic belts highlight the significance of Cretaceous extension and exhumation in shaping the tectonic configuration of the South China Block. Large-scale extension was probably triggered by rollback of the Paleo-Pacific subduction zone.

Key words: Cretaceous extension; delayed exhumation; thermochronology; Mesozoic plateau; Xuefengshan; South China

1. Introduction

This paper presents new thermochronology data for the Xuefengshan Belt (XFSB) of the South China Block (SCB), to explore its exhumation history and how and when Triassic metamorphic belts were modified into their present configurations. We use the results and regional context to propose that a large part of the SCB was an orogenic plateau for much of the Mesozoic, with similarities to modern examples of the Central Andes, Iranian and Tibetan plateaux. The wider aim is to shed light on the evolution of orogenic plateaux in general: they are a major aspect of continental tectonics and growth, but their life cycles are not well-understood. Although the part of the adjacent North China Block has previously been interpreted as an orogenic plateau in the Mesozoic (e.g. Zhang et al., 2008), we are not aware that the SCB has been viewed in this way before.

The XFSB is part of a large Triassic intracontinental fold-and-thrust belt within the southeast and center of the SCB (Fig. 1). Ductile deformation of pre-Late Triassic rocks in the XFSB progressed from the southeastern margin towards the interior of the continent (Li ZX and Li XH, 2007; Chu et al., 2012a; Shu et al., 2015), in response to Paleo-Pacific subduction beneath this margin. Deformation affected other areas of the SCB in the Triassic as the result of collisions along its northern,

northwestern and southern margins (Fig. 1). The area affected by compressional deformation increased through the Jurassic, but without additional collisions at the margins of the SCB. Cretaceous extension formed large continental basins with 2 to 5 km thick terrigenous sedimentary deposits (Fig. 2; Shu et al., 2009; Li JH et al., 2012).

Although exhumation of the XFSB occurred in response to both the Early and Late Mesozoic tectonics of the SCB, the final exhumation and the related thermal evolution history remain poorly understood. This knowledge gap leaves a deficit in our wider understanding of the Mesozoic evolution of the SCB. Our new thermochronology data for the XFSB helps bridge this gap. By comparing cooling paths obtained from different regions of the SCB with our new data, we discuss the widespread delayed exhumation of the Triassic orogens, the implications for Mesozoic tectonics in South China and the more general issue of the relative timing of deformation and exhumation in orogenic belts and plateaux.

2. Geological setting

2.1. The South China Block

The SCB is one of the major continental blocks in East Asia, and consists of the Yangtze and the Cathaysia Blocks to the northwest and southeast, respectively (Fig. 1). The amalgamation of the two blocks occurred in the Neoproterozoic, and gave rise to subduction-collision-related rock formations, including arc-related magmatic and sedimentary rocks between 1.0 and 0.9 Ga (Li, 1999; Li et al., 2009; Wang et al.,

2013, 2016), metamorphic units (1.1-0.9 Ga) (Li et al., 2002, 2007), and post-orogenic intrusions (0.83-0.8 Ga) (Wang et al., 2006; Zheng et al., 2008).

An Early Paleozoic (~460 to 380 Ma) tectonic event interrupted the continuous sedimentation since Late Neoproterozoic times, and strongly reworked the SCB by widespread compression. This intracontinental belt, called the Wuyi-Yunkai orogen, is characterized by amphibolite to granulite facies metamorphism, migmatization, and intensive deformation (Lin et al., 2008; Faure et al., 2009; Li et al., 2010; Chu et al., 2012c, 2014; Shu et al., 2014). A regional Middle to Late Devonian unconformity marks the end of this tectonic event (BGMRJX, 1984, BGMRHN, 1988; Shu et al., 2015).

Deformation affected the entire SCB (Fig. 1) in the Triassic. The Qinling-Dabie-Sulu orogen records Triassic intracontinental subduction of the SCB under the North China Block, and includes one of the largest areas of ultrahigh pressure metamorphic rocks on Earth (Hacker et al., 2000; Meng and Zhang, 2000; Ratschbacher et al., 2000; Faure et al., 2001, 2003). In the southwest, after Permian-Early Triassic South-directed oceanic subduction, the Indochina Block collided with the SCB in the late Early to early Middle Triassic (ca 245-235 Ma) leading to the formation of the Indosinian Orogen (Lepvrier et al., 2004, 2011; Faure et al., 2014, 2016a). In the northwest part of the SCB, Triassic compression was responsible for crustal shortening in the Longmenshan Belt (e. g. Harrowfield and Wilson, 2005; Yan et al., 2011; Xue et al., 2017).

Triassic NW-SE compression formed a broad intracontinental thrust belt from the southeast coastal region of the SCB, to the northwest inland area, in response to the Paleo-Pacific subduction (Wang et al., 2005; Li and Li, 2007; Xu et al., 2011; Chu et al., 2012a, 2012b, 2018; Shu et al., 2015). A flat-slab subduction model has been proposed, which matches the northwest migration of magmatism (Li and Li, 2007). There was a short period in the Late Triassic with post-orogenic magmatism and basin deposition (Li and Li, 2007; Shu et al., 2009). Continental clastic sediments ("molasse") were deposited at the margins of the SCB (e.g. Meng et al., 2005; Qiu et al., 2017). Crustal melt granites produce evidence for major crustal thickening (e.g. He et al., 2010). Later Jurassic and Early Cretaceous compressional tectonics partially reactivated the Triassic belts, and advanced the thrust front westwards to the eastern Sichuan Basin (Li et al., 2018), producing a broad zone of distributed deformation (Fig. 1).

Cretaceous extensional tectonics in the SCB has been recorded in numerous magmatic domes and (half-) graben basins (Fig. 1; Faure et al., 1996; Lin et al., 2000, 2015; Shu et al., 2009; Xu and Wang, 2010; Zhu et al., 2010; Li et al., 2013, 2014; Ji et al., 2018a, 2018b). As a continent-scale response to back-arc extension west of the Paleo-Pacific subduction, Cretaceous extension was coeval with several episodes of magmatic flare-ups (Li XH, 2000; Zhou et al., 2006; Li XH et al., 2010; Li ZX et al., 2012; Li JH et al., 2014; Jiang et al., 2015). In this period, episodic extension and compression alternatively controlled the tectonics of the SCB, suggested to relate to changes of subduction angle of the Paleo-Pacific slab (Zhou et al., 2006; Li et al.,

2010; Li et al., 2014; Jiang et al., 2015; Chu et al., 2018). Extensional domes with detachment zones document at least two episodes of extension-related ductile shearing and exhumation at ~140-120 Ma and ~110-85 Ma, respectively, before and after a short (~10 Myr) compressional event (Webb et al., 1999; Hacker et al., 2000; Lin et al., 2000; Ratschbacher et al., 2000; Zhu et al., 2010; Li et al., 2013, 2016, 2020; Ji et al., 2017, 2018a).

2.2. The Xuefengshan Belt

Located in the center of the SCB, the Xuefengshan Belt (XFSB) is present for >500 km along strike from the NE to the SW (Fig. 2). Although the final establishment of this belt took place in the Late Mesozoic (Dong et al., 2015), the Middle Triassic compressional event accounts for most of the present tectonic architecture. These structures are overlain by a regional Late Triassic-Early Jurassic unconformity (Wang et al., 2005; Chu et al., 2012a, 2012b; Faure et al., 2016b). Beneath Neoproterozoic to Early Triassic non-metamorphic sedimentary formations, a mylonitized décollement zone and its underlying metamorphic rocks correspond to the orogenic cores of the XFSB, which were deformed and metamorphosed between 245 and 225 Ma (Chu et al., 2012a, 2012b). By placing unmetamorphosed rocks over metamorphic rocks, the shear sense of this zone would appear to record an extensional overprinting after the Triassic compressional deformation. Undeformed post-orogenic Middle to Late Triassic granites (~225-215 Ma) intruded into the folded pre-late Triassic strata (Chu et al., 2012c). The XFSB was also deformed by a Late

Jurassic-Early Cretaceous compressional event. This event included the reactivation of previous thrust faults, and the formation of folds and thrusts involving Jurassic sedimentary rocks (Yan et al., 2003; Li et al., 2012; Dong et al., 2015). Unlike the Triassic structures, the Jurassic-Early Cretaceous structures were predominantly formed by brittle deformation. Cretaceous sedimentary basins are bounded by normal faults or detachments and contain several-hundred-meter- to kilometer-thick continental reddish conglomerate, sandstone, and siltstone (EGMRHN, 1988; Shu et al., 2009; Li et al., 2014). On the basin footwalls, the exhumed rocks consist of ductilely deformed and metamorphosed micaschist, or weakly deformed rocks exposed in extensional domes or in horsts bounded by high-angle brittle normal faults, respectively (Li et al., 2013; Ji et al., 2018a; Chu et al., 2019).

3. Deformation in the orogenic core of the Xuefengshan Belt

3.1. Triassic mylonitization (D_1)

The orogenic core of the XFSB is exclusively exposed in the Eastern Zone as two localized domal-shaped metamorphic units, namely the North Orogenic Core (NOC), SW of Xinhua County, and the South Orogenic Core (SOC), East of Chengbu County (Fig. 2). Both the NOC and SOC include micaschist, quartzite, and deformed Early Paleozoic granite, which experienced medium to high greenschist facies metamorphism, pervasive ductile shearing, and mylonitization (Chu et al., 2012b). In the NOC and SOC these Paleozoic granites are the Baimashan and Miaoershan plutons, respectively (Fig. 2).

The SOC shows dominant Triassic ductile deformation characterized by sub-horizontal flat-lying, but undulating foliation (S_1), and NW-SE mineral and stretching lineation (L_1), with a top-to-the NW sense of shear (Figs. 2 and 3a-b; Chu et al., 2012b). The amount of strain in these mylonitized quartzite and two-mica schist is in high contrast with the overlying, weakly metamorphosed and folded sandstone and siltstone. Syn-metamorphic monazite yields U-Th-Pb chemical ages at ~245-225 Ma interpreted as the time of mylonitization (Chu et al., 2012b). The NOC has a dome-shaped structure with NW- or SE-dipping foliation (S_1) and a NW-SE lineation (L_1) formed by a consistent top-to-the NW shearing during the Triassic (Figs. 5a-b). Within the ductile decollement, the Baimaisha pluton was strongly deformed, showing intense mylonitization at its margins.

3.2. Post-Triassic deformation

A distinct late, although weak, tectonic overprint of the Triassic structures is also present. The mylonitic foliation of the décollement zone was strongly crenulated by small upright folds with a wavelength of 0.2 to 1 cm, and 1- to 10 m-scale folds during a late event (Figs. 4a-b). Both the Triassic foliation and lineation are folded by crenulation folds with closely spaced hinge lines (Figs. 4c-d; Chu, 2011). We observe an eastwards decrease in the amount of modification of the primary fabrics in the SOC. Close to the western boundary between the ductile décollement zone and the sedimentary cover, a low-grade metamorphosed pelitic rock is overprinted by strong crenulation, with hinge lines spaced at 0.1-0.5 mm, which could have been initiated in

the fine-grained layers (Fig. 4e). In the center of the SOC, the crenulation is weaker in medium-grade metamorphic rocks. Within two-mica schist, a well-developed crenulation with an obvious northwestward asymmetry only appears in the mica-rich layers, but its 0.5-2 mm wavelength is larger than in the western boundary (Fig. 4f). In the eastern boundary of the décollement zone, the crenulation deformation only generated gently asymmetric small folds with a large wavelength >2 mm (Fig. 4g). Thus, our structural analysis suggests more intense tectonic modification of the D_1 fabrics at the western boundary of the décollement zone than the eastern one. The age of this modification is not clear.

In the NOC, crenulation folded the Triassic foliation in metasedimentary rocks, but barely affected the rigid mylonitized granite (Fig. 5a-b). The S_1 of the micaschist or metapelite is variably modified in this area, and both closely-spaced and widely-spaced crenulation cleavage (S_c) can be observed. This tectonic overprinting is comparable with that of the SOC, suggesting a later event after the Triassic mylonitization during the formation of the XFSB.

4. Sample descriptions

In order to determine the cooling history of the orogenic core of the XFSB, a total of 12 samples were collected, with 10 from the SOC (Figs. 3a and Figs. 4a-f), and 2 from the NOC (Fig. 5).

In the SOC (Fig. 3), we chose an undeformed biotite monzogranite sample XF270 from the Miaoershan pluton that was emplaced at 412 ± 4 Ma (Chu et al.,

2012c). XF270 shows a dominant magmatic texture, but some 0.1-0.5 mm neograins developed at large quartz grain boundaries suggest the initiation of bulging recrystallization (Fig. 4d). Samples XF313 and XF314 are two mylonitic biotite granites from a sheared Early Paleozoic pluton dated at 418 ± 3 Ma in the SOC (Chu, 2012c).

Seven strongly deformed or mylonitized micaschist samples were also selected. Two mylonitic quartz micaschists, XF295 and XF296, and one micaschist XF300 sampled in the north of the SOC include well-crenulated mica-rich layers resulting from a late overprinting (Figs. 4a and 4f). In the center of the SOC, XF316B and XF368 are micaschists deformed by the Triassic ductile shearing and a late crenulation; muscovite/biotite grains are oriented along the mylonitic foliation, but also affected by microscopic folds. In the southern part of the SOC, we collected two garnet micaschist samples, XF312 and XF365, both of which are located close to the décollement zone beneath the Neoproterozoic cover, on the eastern and western flanks of the antiform of the SOC. These micaschists are intensely sheared. Monazite chemical dating of sample XF365 places an age constraint of ~225 Ma on the metamorphism coeval with ductile deformation (Chu et al., 2012b). As noted in section 3, the intensity of crenulation, qualitatively estimated by the microfold wavelength, deceases from west (sample XF365) to east (sample XF312) (Figs. 4e and 4g).

In the NOC, we collected two deformed granite samples, XF224 and XF349 (Fig. 5a). Both samples are biotite monzogranite from the Early Paleozoic Baimashan

pluton, which was emplaced at 411 ± 4 Ma (Chu et al., 2012c). In both samples, field and microscopic observations show similar deformation features, and kinematics. The Triassic synmetamorphic deformation temperature was estimated around 300-400°C from quartz c axis fabrics (Chu et al., 2012b). The late structural superimposition described in section 3 is not observed in this deformed granite.

5. Analytical methods

5.1. ^{40}Ar-^{39}Ar dating

Biotite, muscovite and K-feldspar grains were separated from mylonitic micaschist, quartzite and granites by conventional mineral separation techniques, and handpicked under a binocular microscope to remove visible impurities. Except for samples XF295 and XF365, all ^{40}Ar/^{39}Ar analyses were performed using a MM-5400 mass spectrometer at the ^{40}Ar/^{39}Ar and (U–Th)/He Laboratory, Institute of Geology and Geophysics, Chinese Academy of Sciences (IGGCAS, Beijing). Detailed analytical procedure was described in Wang et al. (2014). Corrections on the measured isotopic ratios were for system blanks, mass discrimination, and irradiation-induced interference. ^{40}Ar/^{39}Ar ages were calculated on ^{40}Ar/^{39}Ar$_K$ ratios and J value from analyses of the monitors and the decay constant. Minerals from sample XF295 and XF365 were processed in Geosciences Montpellier (University of Montpellier). The detailed procedures were described by Monié and Agard (2009). Weighted plateau, inverse isochron and total fusion ages were calculated using the ArArCALC software (Koppers, 2002). Age data are presented with 2-sigma

uncertainties. For analyses on K-feldspar, the various model parameters, e.g. active energy and relative domain size were processed with appropriate adjustment. Multi-domain diffusion modeling was conducted to obtain a modeled age spectrum and cooling history.

5.2. (U-Th)/He dating

Zircon and apatite separation were conducted in the same procedure as for mica and feldspar. We performed the analyses at the $^{40}Ar/^{39}Ar$ and (U–Th)/He Laboratory, Institute of Geology and Geophysics, Chinese Academy of Sciences (IGGCAS, Beijing). Euhedral apatite and zircon grains were handpicked for inclusion-free grains under a high-power microscope, and then packaged in Pt (for apatite) and Nb (for zircon) microtubes for (U-Th)/He dating analysis. Detailed parameters and procedures were presented by Wu et al. (2016) and Shi et al. (2018). Standard minerals were used to verify the analytical procedure: Durango apatite (dated at 32.2 ± 1.0 Ma by Wu et al., 2016, and 31.9 ± 1.2 Ma by Reiners and Nicolescu, 2006), and Fish Canyon Tuff zircon (dated at 28.3 ± 2.6 Ma; Reiners, 2005).

6. Results

We obtained 11 ^{40}Ar-^{39}Ar results on biotite or muscovite, and 2 on K-feldspar by conventional step-heating method (Figs. 5 and 6; Tables S1-S3). The age spectra for mica are shown in Figs. 7 and 8, and K-feldspar analytical and modeled age

spectra and cooling paths are shown in Fig. 9. We also acquired 3 zircon (U-Th)/He (ZHe) and 2 apatite (U-Th)/He (AHe) ages (Tables S4 and S5).

6.1. Mica ^{40}Ar-^{39}Ar dating

All mica dating results are within the age range 150-88 Ma, and 10 ages are clustered in the Early Cretaceous (Figs. 7 and 8; Table S1 and S2). Initial ^{40}Ar/^{36}Ar ratios are calculated for all samples, whereas those of XF233 and XF365 are poorly constrained due to the narrow range of their ^{40}Ar/^{39}Ar ratios (Table S2). All the initial ^{40}Ar/^{36}Ar ratios are close to 295, indicating negligible excess argon in the dated minerals (Table S1). Except for XF300 and XF314, all samples have weighted plateau ages that are consistent with their total fusion ages and inverse isochron ages within errors (Figs. 7 and 8). The weighted plateau age (107.9 ± 3.6 Ma) of sample XF314 is ~10 Myr younger than its total fusion age (119.6 ± 3.4 Ma), whereas XF300 has a rugged age spectrum associated with different amounts of released ^{39}Ar. Indeed, most samples show uneven age spectra, possibly indicating a later thermal perturbation.

In the SOC, undeformed granite sample XF270 from the Miaoershan pluton yields a biotite ^{40}Ar-^{39}Ar weighted plateau age at 143.4 ± 3.4 Ma (Fig. 7a). Two sheared granite samples XF313 and XF314 are dated at 124.8 ± 5.7 Ma and 116.8 ± 1.2 Ma respectively (Figs. 7d-e). Ages from micaschists vary in a more concentrated range at 132-136 Ma, but sample XF300 gives a much younger total fusion age of 108.8 ± 1.4 Ma. Sample XF224 from the NOC yields a late Cretaceous age of ~88 Ma (Fig. 7h).

6.2. K-feldspar ^{40}Ar-^{39}Ar results and multi-domain diffusion modelling

Two K-feldspar samples, XF270 from the Miaoershan pluton, and XF349 from the Baimashan pluton, have been analyzed by the high-resolution ^{40}Ar-^{39}Ar step-heating method (McDougall and Harrison, 1999). The multi-domain diffusion model of the ^{40}Ar-^{39}Ar system in K-feldspar is the most widely used method for reconstructing the thermal evolution at 150-350°C (Lovera et al., 1997, 2002; McDougall and Harrison, 1999).

Both samples show several rugged steps at low temperatures because of excess Ar present in the margin of the mineral. The age spectra of sample XF270 range from 56 Ma to 164 Ma with a total fusion age of 121 Ma (Fig. 9a), which is close to its biotite ^{40}Ar-^{39}Ar age. A small age plateau is shown around 128 Ma with 18% of the total released argon, suggesting a rapid cooling event at this time. Cooling history demonstrates a fast cooling from 155 Ma to 125 Ma, and fits well with the total fusion age and the weighted plateau age (Fig. 9b). Another cooling stage at 50-40 Ma is indicated at the end of this curve, but it has low reliability because the majority of the curve is in the low-temperature domain (<150°C).

Sample XF349 has age spectra between 116 Ma and 289 Ma with a total fusion age at 222 Ma (Fig. 9c). The relatively flat portion with 22% of the total released argon yields a weighted plateau age at ~221 Ma in agreement with the total fusion age. Multi-domain diffusion modeling reveals two stages of fast cooling; one from 255 Ma

to 220 Ma that complies with the total fusion age and the weighted plateau age, and the other from 105 Ma to 80 Ma (Fig. 9d).

6.3. (U-Th)/He dating

All samples for ZHe and AHe dating are collected from the SOC (Fig. 6). ZHe ages from samples XF296, XF313, and XF368 range from 100 Ma to 77 Ma. XF296 has a Late Cretaceous AHe age of 78 Ma. Thus, according to the closure temperatures for ZHe and AHe of 185 ± 10°C, and 65 ± 5°C, respectively (Wolf et al., 1996; Farley, 2002; Reiners et al., 2002; Reiners, 2005), these results show that the southern core of the XFSB experienced relatively fast cooling, at a rate at ~8°C/Myr during the Late Cretaceous. In contrast, sample XF368 yields a Late Jurassic AHe age with large uncertainties, that is older than the ZHe age of this sample. Considering the ^{40}Ar-^{39}Ar ages that are exclusively younger than 150 Ma, the AHe age of XF368 likely reflects a mixed result due to partial resetting on the isotopic system.

7. Discussion

7.1. Tectonothermal history of the Xuefengshan Belt

Previous structural studies have demonstrated the dominance of Triassic tectonics in the development of the XFSB (Wang et al., 2005; Chu et al., 2012a, 2015). Recent work on the ductile décollement zone gives an Early Triassic age (ca. 245-225 Ma) for the syn-tectonic metamorphism of the garnet-micaschist (Chu, 2011; Chu et al., 2012b). In the NOC, our new data clearly indicate this Early Triassic

tectono-thermal event underwent a 2-3°C/Myr cooling gradient in the modeled thermal history of the Baimashan pluton (Fig. 9b). The thermal history for the Baimashan pluton also documents a fast cooling at ~100-85 Ma, consistent with the biotite ^{40}Ar-^{39}Ar age at ~88 Ma (Fig. 9b).

In the SOC, structural observations reveal a second deformation phase that reworked the Triassic structures by pervasive crenulation cleavages. The development of these crenulations was coeval with a low-temperature overprint of the previous structures as the result of reactivation along the décollement zone. Our thermochronology results indicate that the overprint took place in the Late Jurassic-Early Cretaceous, and may have reached a peak at ~130 Ma, as documented by the ^{40}Ar-^{39}Ar ages (Fig. 9). Indeed, the Cretaceous event observed in the SOC has a similar timing and style to the extensional tectonics in the adjacent Yuechengling pluton, where a large-scale detachment accommodated extensional exhumation of the dome structure (Chu et al., 2019). In the northwest part of the XFSB, Cretaceous extension also formed large continental basins with shallow to semi-deep lake facies deposits (Tang et al., 2014).

The K-feldspar modeled cooling history from the undeformed part of the Miaoershan pluton shows that a fast cooling stage began at ~160 Ma, and lasted until ~130 Ma, at an overall exhumation rate of ~4°C/Myr (Fig. 9). In the XFSB, the late Jurassic-earliest Cretaceous compression is followed by Early Cretaceous extension (BGMRHN, 1988; Shu et al., 2009; Li et al., 2014), but the transition between compression and extension are still debated (Zhou and Li, 2000; Dong et al., 2008,

2015). The incipient cooling of the Miaoershan pluton at ~160 Ma (ca. 10 Myr earlier than the earliest ^{40}Ar-^{39}Ar age recorded in the SOC), took place in a transitional stage between the Middle-Late Jurassic extension, and the Late Jurassic-Early Cretaceous regional compression of the SCB (Zhou and Li, 2000; Li et al., 2014).

Metamorphic rocks from the SOC do not yield any Late Cretaceous ^{40}Ar-^{39}Ar ages, which suggests they were already at upper crustal depths before the second phase of exhumation at this time (Fig. 10). ZHe and AHe ages provide a well-constrained cooling pattern in which fast cooling from ~7 ± 1 km to ~3 ± 1 km occurred at ~100-80 Ma in the SOC, but Late Cretaceous exhumation of the NOC began at a deeper level, at depths of ~12 ± 2 km (assuming an average paleo-temperature gradient of 25°C/km).

To summarize, the NOC records an Early Triassic thermal event, overprinted by a Late Cretaceous cooling event, whereas the SOC shows a two-stage cooling path in the Early and Late Cretaceous periods (Fig. 10). In spite of the internal variations during the exhumation, the XFSB experienced a two-stage exhumation in the Late Mesozoic: one from ~150 Ma to 110 Ma, centered at ~130 Ma, and another one between ~100-80 Ma (Fig. 9). The two-stage exhumation pattern is also identified in the adjacent regions of the XFSB. To the SE of the SOC, the Yuechengling pluton, (Fig. 2), preserved two phases of ductile extensional deformation that took place at 140-120 Ma and 100-85 Ma respectively (Chu et al., 2019). The Hengshan detachment initiated in the Early Cretaceous (Fig. 2), and was followed by a Late Cretaceous cooling event (Li et al., 2013; Wei et al., 2016). Fault slip analysis in the

Yuanma Basin also demonstrates two stages of ~NW-SE extension in the Early and Late Cretaceous, respectively (Li et al., 2012). Therefore, all of these lines of evidence support a two-stage extensional history across the XFSB in the Late Mesozoic, principally in the Early and Late Cretaceous (Fig. 10).

7.2. Regional Cretaceous exhumation of Triassic orogens: implications for the destruction of the Mesozoic plateau in South China

Triassic tectonics had a major impact across the SCB, creating a wide intracontinental fold-and-thrust belt that probably resembled an Andean-type orogenic plateau, superimposed on the crustal thickening caused by the continental collisions along its northern and southern margins (Yin and Nie, 1996; Li and Li, 2007; Chu et al., 2012a). During the Late Triassic to Early Jurassic, A-type and basaltic magmatism implies signatures of the asthenospheric mantle, but the Triassic orogenic plateau was preserved during the following compression (Li et al., 2014).

We propose a model that regional exhumation and destruction of this plateau occurred in the Cretaceous, and here review the regional evidence that supports this model (Fig. 11). At the northern margin of the SCB, post-orogenic extension of the Early Mesozoic high pressure–ultrahigh pressure Qinling-Dabieshan-Sulu belt gave rise to a fast cooling phase in the Late Triassic-Early Jurassic (Figs. 1 and 11), but the Early Cretaceous large-scale extension also exposed a large portion of the exposed UHP and high temperature metamorphic units at 130-120 Ma (Ratschbacher et al., 2000; Lin et al., 2015; Ji et al., 2017). As the western extension of the Dabieshan belt,

the Triassic Tongbaishan belt was also overprinted by two stages of ductile extension that exhumed a large portion of the high pressure rocks during the Early and Late Cretaceous eras (Fig. 11a) (Webb et al., 1999; Liu et al., 2010; Xu and Wang, 2010; Cui et al., 2012).

Our new results argue for similar Cretaceous overprinting of the Triassic XFSB (Fig. 11b). The décollement zone that represents the orogenic core of this belt developed during the Early Triassic, but its final exhumation to the upper crustal or subaerial level was completed in the Late Cretaceous, following an Early Cretaceous stage of exhumation (Fig. 11b). In the southern part of the SCB, the Triassic orogenic events deformed the early Paleozoic deformed and metamorphosed rocks in the Yunkai, Baiyunshan, and Song Chay Massifs (Fig. 1; Roger et al., 2000; Wang et al., 2007; Wan et al., 2010; Chen et al., 2011, 2017), while the Cretaceous extension exhumed the Triassic basement with a fast cooling stage at ~140-120 Ma (Fig. 11b), and played an important role in the formation of the present orogenic configuration (Roger et al., 2000; Yang et al., 2010).

Delayed exhumation of the Triassic orogenic belts appears to be a common phenomenon across the SCB (Fig. 12). Despite variations in exhumation rates and patterns, this widespread Cretaceous extension shows a connection to continental-scale extensional tectonics induced by Paleo-Pacific subduction (Fig. 12b; Li XH, 2000; Zhou and Li, 2000; Li and Li, 2007; Li JH et al., 2014; Ji et al., 2018a). The crust of the North China Block was profoundly extended in numerous metamorphic core complexes and (half-) graben basins in a short period at 130-120

Ma. At depth, the NCB lithospheric mantle was also removed by effects of the Paleo-Pacific subduction (Lin and Wang, 2006; Wu et al., 2019). The SCB may have evolved under a contrasting regime. After the formation of the Triassic belts, a significant portion of orogenic cores, such as the XFSB, remained stagnant at the upper-middle crustal level (Fig. 10). Although compressional deformation may have played a role in the Jurassic tectonics of the SCB (Dong et al., 2008, 2015; Shu et al., 2009; Li et al., 2014), it had had limited impact on the cooling paths from the pre-existing Triassic belts. The Triassic orogenic core units retained their position in the crust (Figs. 10 and 11). In the Cretaceous, the long-lasting, episodic extension facilitated the exhumation of these orogenic cores, most of which were exposed to their present, subaerial levels, as shown by metamorphosed/deformed pebbles in the Cretaceous basins (Fig. 12; Zhang et al., 2010; Chu et al., 2019).

The Triassic SCB probably resembled other orogenic plateaux (Fig. 13), such as the North American Cordillera ("Nevadaplano") in the Late Mesozoic (Dickinson, 2004; Yonkee and Weil, 2015), the Late Cretaceous Lhasa terrane ("Lhasaplano"; Kapp et al., 2007; Wang et al., 2017), or the Cenozoic Central Andes (Altiplano and Puna plateaux; Espurt et al., 2008). All these regions are characterized by retroarc fold-and-thrust belts, which thickened the crust over broad regions. However, these plateaux have had different fates. The Nevadaplano was dismantled during Late Cenozoic extension (Colgan and Henry, 2009). The high elevation of the Lhasaplano was preserved because of the subsequent India-Eurasia collision that persisted or enhanced the compression (Wang et al., 2017). The Central Andean Plateau was built

by compressional deformation since ~40 Ma, and is still growing laterally and across strike (McQuarrie et al., 2008; Scott et al., 2018).

The implication of our study on the SCB plateau is that the other orogenic plateaux may have experienced (or will experience) similar long time lags between the construction of the belt, and widespread destruction by extension and exhumation of rocks to surface or near-surface levels. It is notable that this scenario implies little or no denudation throughout the Jurassic for the SCB, in keeping with the lack of evidence for exhumation or tectonic deformation through this period, with the implication that erosional processes on their own were not sufficient to reduce the Triassic plateau to near-normal crustal thicknesses and elevation.

Taking the present regional crustal thickness of the interior of the SCB as ~35 km (He et al., 2014), and adding ~10 km as a very rough estimate of regional exhumation by the end of the Cretaceous, gives an indicative Triassic crustal thickness of ~45 km. While this figure is much less than crustal thicknesses in the modern Andean or Tibetan plateaux, it is comparable with the interior of the Iranian Plateau (Taghizadeh-Farahmand et al., 2015), and suggests that regional paleo-elevations may have been on the order of 1.5 km above sea level, by analogy with the modern Iranian plateau.

Present lateral dimensions of the paleo-SCB plateau are ~1300 km northeast-southwest from the Qinling-Dabie-Sulu belts in the northeast to the Indosinian Orogen in the southwest (Fig. 1). The northwest-southeast dimension is harder to reconstruct, but potentially reached from the western margin of the

Xuefengshan deep into the interior of the Cathaysia Block, which is a present-day distance of ~500 km (Fig. 1). The total area involved is therefore ~800,000 km^2. This is comparable to the Central Andean Plateau, but smaller than the Turkish-Iranian or Tibetan plateaux (~1,400,000 and 2,000,000 km^2 respectively). The paleo-SCB plateau should have been wider before the Cretaceous extension, but the initial width is unknown as the extension factor is not yet constrained.

8. Conclusions

A complex cooling path is recorded in the orogenic core of the XFSB. In this belt, Early Triassic ductile deformation produced a greenschist to lower amphibolite facies décollement zone overlying two orogenic cores. The northern core underwent Late Triassic extension, whereas the southern orogenic core retained its middle crustal position through this time. Both cores underwent significant Cretaceous exhumation, but in different ways. The southern orogenic core had a two-stage exhumation process, with Early Cretaceous exhumation to ~7 ± 1 km depth, and Late Cretaceous exhumation to ~3 ± 1 km depth. The northern orogenic core only underwent the Late Cretaceous stage that exhumed the rocks from ~12 ± 2 km to ~6 ± 1 km depth (Fig. 10). Combining the available evidence leads us to propose that the larger part of the SCB was an orogenic plateau from its construction in the Late Triassic until its destruction in the Late Cretaceous. This concept is no doubt a great simplification of a complex region, but it gives a new framework for understanding each facet of the geology.

Comparison with other Triassic orogenic belts of the SCB (Fig. 11) indicates that such postponed exhumation may be a common phenomenon. Although the detailed exhumation history for each belt varies (Fig. 13), we emphasize the common importance of Cretaceous extension in the SCB, that established the present structure. Changes in stress state at the Paleo-Pacific plate boundary are the most likely cause of Cretaceous extension (Fig. 12), following a long period where an orogenic plateau of thick continental crust remained in equilibrium, neither collapsing nor enlarging.

Acknowledgements

This study was funded by the Ministry of Science and Technology (2016YFC0600401 and 2016YFC0600102), the National Natural Science Foundation of China (91855212, 41872208, and 41302161), the China Scholarship Council (201804910283), and the Youth Innovation Promotion Association. T. Francois, an anonymous reviewer, and Editor Phillipe Agard are acknowledged for their constructive comments and suggestions. Mr. J.Y. Li is thanked for his help during the fieldwork, and Drs. P. Monié, L. Wu, and W.B. Shi are thanked for their assistance in the Ar-Ar and (U-Th)/He analysis. This work also benefited from the discussions in Coffice 442 of the Institute of Geology and Geophysics, Chinese Academy of Sciences.

References

Bureau of Geology and Mineral Resources of Hunan province (BGMRHN), 1988.

Regional Geology of the Hunan Province. Geological Publishing House, Beijing. 507 pp.

Bureau of Geology and Mineral Resources of Jiangxi Province (BGMRJX), 1984. Regional Geology of the Jiangxi Province. Geological Publishing House, Beijing. 921 pp.

Chen, C.-H., Hsieh, P.-S., Lee, C.-Y., Zhou, H.-W., 2011. Two episodes of the Indosinian thermal event on the South China Block: Constraints from LA-ICPMS U-Pb zircon and electron microprobe monazite ages of the Darongshan S-type granitic suite. Gondwana Res. 19, 1008-1023.

Chen, C.-H., Liu, Y.-H., Lee, C.-Y., Xiang, H., Zhou, H.-W., 2012. Geochronology of granulite, charnockite and gneiss in the poly-metamorphosed Gaozhou Complex (Yunkai massif), South China: Emphasis on the in-situ EMP monazite dating. Lithos 144–145, 109-129.

Chen, C.-H., Liu, Y.-H., Lee, C.-Y., Sano, Y., Zhou, H.-W., Xiang, H., Takahata, N., 2017. The Triassic reworking of the Yunkai massif (South China): EMP monazite and U-Pb zircon geochronologic evidence. Tectonophysics 694, 1-22.

Chu, Y., Faure, M., Lin, W., Wang, Q., 2012a. Early Mesozoic tectonics of the South China block: Insights from the Xuefengshan intracontinental orogen. J Asian Earth Sci 61, 199-220.

Chu, Y., Faure, M., Lin, W., Wang, Q., Ji, W., 2012b. Tectonics of the Middle Triassic intracontinental Xuefengshan Belt, South China: new insights from structural and chronological constraints on the basal décollement zone. Int J Earth Sci 101,

2125-2150.

Chu, Y., Lin, W., Faure, M., Wang, Q., Ji, W., 2012c. Phanerozoic tectonothermal events of the Xuefengshan Belt, central South China: Implications from U-Pb age and Lu-Hf determinations of granites. Lithos 150, 243-255.

Chu, Y., Lin, W., 2014. Phanerozoic polyorogenic deformation in southern Jiuling Massif, northern South China block: Constraints from structural analysis and geochronology. J Asian Earth Sci 86, 117-130.

Chu, Y., Lin, W., Faure, M., Wang, Q., 2015. Early Mesozoic intracontinental orogeny: Example of the Xuefengshan-Jiuling Belt. Acta Petrol Sin 31, 2145-2155.

Chu, Y., Lin, W., 2018. Strain analysis of the Xuefengshan Belt, South China: From internal strain variation to formation of the orogenic curvature. J Struct Geol 116, 131-145.

Chu, Y., Lin, W., Faure, M., Xue, Z., Ji, W., Wu, L., Feng, Z., 2019. Cretaceous episodic extension in South China Block, East Asia: Evidence from the Yuechengling Massif of central South China. Tectonics, 38. https://doi.org/10.1029/2019TC005516.

Colgan, J.P., Henry, C.D., 2009. Rapid middle Miocene collapse of the Mesozoic orogenic plateau in north-central Nevada. Int. Geol. Rev. 51, 920-961.

Cui, J., Liu, X., Dong, S., Hu, J., 2012. U–Pb and 40Ar/39Ar geochronology of the Tongbai complex, central China: Implications for Cretaceous exhumation and lateral extrusion of the Tongbai–Dabie HP/UHP terrane. J Asian Earth Sci 47, 155-170.

Dickinson, W.R., 2004. Evolution of the North American Cordillera. Annu Rev Earth Planet Sci 32, 13-45.

Ding, X., Chen, P.R., Chen, W.F., Huang, H.Y., Zhou, X.M., 2005. LA-ICPMS zircon U\Pb age determination of the Weishan granite in Hunan: petrogenesis and significance. Science in China (D) 35, 606–616.

Dong, S., Zhang, Y., Long, C., Yang, Z., Ji, Q., Wang, T., Hu, J., Chen, X., 2008. Jurassic tectonic revolution in China and new interpretation of the "Yanshan Movement". Acta Geol. Sin. 82, 334-347.

Dong, S., Zhang, Y., Zhang, F., Cui, J., Chen, X., Zhang, S., Miao, L., Li, J., Shi, W., Li, Z., Huang, S., Li, H., 2015. Late Jurassic–Early Cretaceous continental convergence and intracontinental orogenesis in East Asia: A synthesis of the Yanshan Revolution. J. Asian Earth Sci 114, 750-770.

Espurt, N., Funiciello, F., Martinod, J., Guillaume, B., Regard, V., Faccenna, C., Brusset, S., 2008. Flat subduction dynamics and deformation of the South American plate: Insights from analog modeling. Tectonics 27, TC3011, 10.1029/2007tc002175.

Farley, K. A. (2002). (U-Th)/He dating: Techniques, calibrations, and applications, Reviews in Mineralogy and Geochemistry, 47, 819–844. https://doi.org/10.2138/rmg.2002.47.18.

Faure, M., Sun, Y., Shu, L., Monié, P., Charvet, J., 1996. Extensional tectonics within a subduction-type orogen. The case study of the Wugongshan dome (Jiangxi Province, southeastern China). Tectonophysics 263, 77-106.

Faure, M., Lin, W., Shu, L.S., Sun, Y., Scharer, U., 1999. Tectonics of the Dabieshan (eastern China) and possible exhumation mechanism of ultra high-pressure rocks. Terra Nova 11, 251-258.

Faure, M., Lin, W., Le Breton, N., 2001. Where is the North China-South China block boundary in eastern China? Geology 29, 119-122.

Faure, M., Lin, W., Scharer, U., Shu, L.S., Sun, Y., Arnaud, N., 2003. Continental subduction and exhumation of UHP rocks. Structural and geochronological insights from the Dabieshan (East China). Lithos 70, 213-241.

Faure, M., Shu, L., Wang, B., Charvet, J., Choulet, F., Monie, P., 2009. Intracontinental subduction: a possible mechanism for the Early Palaeozoic Orogen of SE China. Terra Nova 21, 360-368.

Faure, M., Lepvrier, C., Nguyen, V.V., Vu, T.V., Lin, W., Chen, Z., 2014. The South China block-Indochina collision: Where, when, and how? J Asian Earth Sci 79, 260-274.

Faure, M., Lin, W., Chu, Y., Lepvrier, C., 2016a. Triassic tectonics of the Ailaoshan Belt (SW China): Early Triassic collision between the South China and Indochina Blocks, and Middle Triassic intracontinental shearing. Tectonophysics 683, 27-42.

Faure, M., Lin, W., Chu, Y., Lepvrier, C., 2016b. Triassic tectonics of the southern margin of the South China Block. C.R. Geosci. 348, 5-14.

François, T., Agard, P., Bernet, M., Meyer, B., Chung, S.L., Zarrinkoub, M.H., Burov, E., Monié, P., 2014. Cenozoic exhumation of the internal Zagros: first

constraints from low-temperature thermochronology and implications for the build-up of the Iranian plateau. Lithos 206-207, 100-112.

Hacker, B.R., Ratschbacher, L., Webb, L., McWilliams, M.O., Ireland, T., Calvert, A., Dong, S.W., Wenk, H.R., Chateigner, D., 2000. Exhumation of ultrahigh-pressure continental crust in east central China: Late Triassic-Early Jurassic tectonic unroofing. Journal of Geophysical Research-Solid Earth 105, 13339-13364.

Harrowfield, M. J., Wilson, C. J. L., 2005. Indosinian deformation of the Songpan Ganze Fold Belt, northeast Tibetan Plateau. J. Struct. Geol., 27, 101–117.

Harrison, T.M., Copeland, P., Kidd, W.S.F. and Yin, A., 1992. Raising Tibet. Science 255, 1663-1670.

He, Z.Y., Xu, X.S., Niu, Y.L., 2010. Petrogenesis and tectonic significance of a Mesozoic granite–syenite–gabbro association from inland South China. Lithos 119, 621-641.

He, R., Shang, X., Yu, C., Zhang, H. and Van der Hilst, R.D., 2014. A unified map of Moho depth and Vp/Vs ratio of continental China by receiver function analysis. Geophysical Journal International, 199(3): 1910-1918.

Isacks, B. L. (1988), Uplift of the Central Andean Plateau and bending of the Bolivian Orocline, Journal of Geophysical Research-Solid Earth and Planets, 93(B4), 3211-3231.

Ji, W., Lin, W., Faure, M., Shi, Y., Wang, Q., 2017. The early Cretaceous orogen-scale Dabieshan metamorphic core complex: implications for extensional collapse of

the Triassic HP–UHP orogenic belt in east-central China. Int J Earth Sci 106, 1311-1340.

Ji, W., Faure, M., Lin, W., Chen, Y., Chu, Y., Xue, Z., 2018a. Multiple Emplacement and Exhumation History of the Late Mesozoic Dayunshan-Mufushan Batholith in Southeast China and Its Tectonic Significance: 1. Structural Analysis and Geochronological Constraints. Journal of Geophysical Research: Solid Earth 113, 689-710.

Ji, W., Chen, Y., Chen, K., Wei, W., Faure, M., Lin, W., 2018b. Multiple Emplacement and Exhumation History of the Late Mesozoic Dayunshan-Mufushan Batholith in Southeast China and Its Tectonic Significance: 2. Magnetic Fabrics and Gravity Survey. Journal of Geophysical Research: Solid Earth 113, 711-731.

Jiang, X.-Y., Li, X.-H., Collins, W.J., Huang, H.-Q., 2015. U-Pb age and Hf-O isotopes of detrital zircons from Hainan Island: Implications for Mesozoic subduction models. Lithos 239, 60-70.

Kapp, P., DeCelles, P.G., Leier, A.L., Fabijanic, J.M., He, S., Pullen, A., Gehrels, G.E., Ding, L., 2007. The Gangdese retroarc thrust belt revealed. GSA Today 17, 4.

Koppers, A. A. P., 2002. ArArCALC—Software for 40Ar/39Ar age calculations. Computer & Geosciences, 28, 605–619, doi:10.1016/S0098-3004(01)00095-4.

Law, R., Allen, M.B., 2020. Diachronous Tibetan Plateau landscape evolution derived from lava field geomorphology. Geology 48, 263-267.

Lepvrier, C., Maluski, H., Van Tich, V., Leyreloup, A., Truong Thi, P., Van Vuong, N., 2004. The Early Triassic Indosinian orogeny in Vietnam (Truong Son Belt and

Kontum Massif); implications for the geodynamic evolution of Indochina. Tectonophysics 393, 87-118.

Lepvrier, C., Van Vuong, N., Maluski, H., Truong Thi, P., Van Vu, T., 2008. Indosinian tectonics in Vietnam. Comptes Rendus Geosciences 340, 94-111.

Lepvrier, C., Faure, M., Van, V.N., Vu, T.V., Lin, W., Trong, T.T., Hoa, P.T., 2011. North-directed Triassic nappes in Northeastern Vietnam (East Bac Bo). J Asian Earth Sci 41, 56-68.

Li, Y.H., Gao, M.T., Wu, Q.Y., 2014. Crustal thickness map of the Chinese mainland from teleseismic receiver functions. Tectonophysics 611, 51-60.

Li, J., Zhang, Y., Dong, S., Li, H., 2012. Late Mesozoic–Early Cenozoic deformation history of the Yuanma Basin, central South China. Tectonophysics 570–571, 163-183.

Li, J., Zhang, Y., Dong, S., Su, J., Li, Y., Cui, J., Shi, W., 2013. The Hengshan low-angle normal fault zone: Structural and geochronological constraints on the Late Mesozoic crustal extension in South China. Tectonophysics 606, 97-115.

Li, J., Zhang, Y., Dong, S., Johnston, S.T., 2014. Cretaceous tectonic evolution of South China: A preliminary synthesis. Earth-Science Reviews 134, 98-136.

Li, J., Dong, S., Zhang, Y., Zhao, G., Johnston, S.T., Cui, J., Xin, Y., 2016. New insights into Phanerozoic tectonics of south China: Part 1, polyphase deformation in the Jiuling and Lianyunshan domains of the central Jiangnan Orogen. Journal of Geophysical Research: Solid Earth 121, 3048-3080.

Li, J., Dong, S., Cawood, P.A., Zhao, G., Johnston, S.T., Zhang, Y., Xin, Y., 2018. An

Andean-type retro-arc foreland system beneath northwest South China revealed by SINOPROBE profiling. Earth Planet Sci Lett 490, 170-179.

Li, J., Cawood, P.A., Ratchbacher, L., Zhang, Y., Dong, S., Xin, Y., Yang, H., Zhang, P., 2020. Building Southeast China in the late Mesozoic: Insights from alternating episodes of shortening and extension along the Lianhuashan fault zone. Earth Science Reviews 201, 103056.

Li, S., Santosh, M., Zhao, G., Zhang, G. and Jin, C., 2011. Intracontinental deformation in a frontier of super-convergence: A perspective on the tectonic milieu of the South China Block. Journal of Asian Earth Sciences, 49: 313-329.

Li, X.H., 1999. U-Pb zircon ages of granites from the southern margin of the Yangtze Block: timing of Neoproterozoic Jinning: Orogeny in SE China and implications for Rodinia Assembly. Precambrian Res 97, 43-57.

Li, X.-H., 2000. Cretaceous magmatism and lithospheric extension in Southeast China. J Asian Earth Sci 18, 293-305.

Li, X.-H., Li, W.-X., Li, Z.-X., Lo, C.-H., Wang, J., Ye, M.-F., Yang, Y.-H., 2009. Amalgamation between the Yangtze and Cathaysia Blocks in South China: Constraints from SHRIMP U-Pb zircon ages, geochemistry and Nd-Hf isotopes of the Shuangxiwu volcanic rocks. Precambrian Res 174, 117-128.

Li, X.H., Li, W.X., Wang, X.C., Li, Q.L., Liu, Y., Tang, G.Q., Gao, Y.Y., Wu, F.Y., 2010. SIMS U-Pb zircon geochronology of porphyry Cu-Au-(Mo) deposits in the Yangtze River Metallogenic Belt, eastern China: Magmatic response to early Cretaceous lithospheric extension. Lithos 119, 427-438.

Li, Z.X., Li, X.H., Zhou, H.W., Kinny, P.D., 2002. Grenvillian continental collision in south China: New SHRIMP U-Pb zircon results and implications for the configuration of Rodinia. Geology 30, 163-166.

Li, Z.X., Li, X.H., 2007. Formation of the 1300-km-wide intracontinental orogen and postorogenic magmatic province in Mesozoic South China: A flat-slab subduction model. Geology 35, 179-182.

Li, Z.X., Wartho, J.A., Occhipinti, S., Zhang, C.L., Li, X.H., Wang, J., Bao, C.M., 2007. Early history of the eastern Sibao Orogen (South China) during the assembly of Rodinia: New mica Ar-40/Ar-39 dating and SHRIMP U-Pb detrital zircon provenance constraints. Precambrian Res 159, 79-94.

Li, Z.-X., Li, X.-H., Wartho, J.-A., Clark, C., Li, W.-X., Zhang, C.-L., Bao, C., 2010. Magmatic and metamorphic events during the early Paleozoic Wuyi-Yunkai orogeny, southeastern South China: New age constraints and pressure-temperature conditions. Geol Soc Am Bull 122, 772-793.

Li, Z.-X., Li, X.-H., Chung, S.-L., Lo, C.-H., Xu, X., Li, W.-X., 2012. Magmatic switch-on and switch-off along the South China continental margin since the Permian: Transition from an Andean-type to a Western Pacific-type plate boundary. Tectonophysics 532-535, 271-290.

Lin, W., Faure, M., Monie, P., Scharer, U., Zhang, L.S., Sun, Y., 2000. Tectonics of SE China: New insights from the Lushan massif (Jiangxi Province). Tectonics 19, 852-871.

Lin, W., Wang, Q.C., 2006. Late Mesozoic extensional tectonics in the North China

block: a crustal response to subcontinental mantle removal? Bull Soc Geol Fr 177, 287-297.

Lin, W., Wang, Q., Chen, K., 2008. Phanerozoic tectonics of south China block: New insights from the polyphase deformation in the Yunkai massif. Tectonics 27.

Lin, W., Shi, Y., Wang, Q., 2009. Exhumation tectonics of the HP-UHP orogenic belt in Eastern China: New structural-petrological insights from the Tongcheng massif, Eastern Dabieshan. Lithos 109.

Lin, W., Ji, W., Faure, M., Wu, L., Li, Q., Shi, Y., Schaer, J., Wang, F., Wang, Q., 2015. Early Cretaceous extensional reworking of the Triassic HP–UHP metamorphic orogen in Eastern China. Tectonophysics 662, 256-270.

Lin, W., Wei, W., 2019. Late Mesozoic extensional tectonics in the North China Craton and its adjacent regions: a review and synthesis. Int Geo Rev, https://doi.org/10.1080/00206814.2018.1477073.

Liu, X., Jahn, B.-m., Cui, J., Li, S., Wu, Y., Li, X.-h., 2010. Triassic retrograded eclogites and Cretaceous gneissic granites in the Tongbai Complex, central China: Implications for the architecture of the HP/UHP Tongbai–Dabie–Sulu collision zone. Lithos 119, 211-237.

Lovera, O.M., Grove, M., Harrison, T.M., Mahon, K.I., 1997. Systematic analysis of K- feldspar 40Ar/39Ar step heating results: I. Significance of activation energy determinations. Geochimica et Cosmochimica Acta 61, 3171–3192.

Lovera, O.M., Grove, M., Harrison, T.M., 2002. Systematic analysis of K-feldspar 40Ar/39Ar step heating results II: Relevance of laboratory argon diffusion

properties to nature. Geochimica et Cosmochimica Acta 66, 1237–1255.

Magni, V., Allen, M.B., van Hunen, J. and Bouilhol, P. 2017. Continental underplating after slab break-off, Earth and Planetary Science Letters, 474, 59 –67.

McDougall, I., Harrison, T.M., 1999. Geochronology and Thermochronology by the 40Ar/39Ar Method. Oxford University Press, Oxford, pp. 1–269.

McQuarrie, N., Barnes, J. B., and Ehlers, T. A. 2008. Geometric, kinematic, and erosional history of the central Andean Plateau, Bolivia (15 – 17°S), Tectonics, 27, TC3007, doi:10.1029/2006TC002054.

Meng, Q. R., and Zhang, G.W., 2000., Geologic framework and tectonic evolution of the Qinling orogen, central China. Tectonophysics, 323, 183–196.

Meng, Q.-R., Wang, E. and Hu, J.-M. 2005. Mesozoic sedimentary evolution of the northwest Sichuan basin: Implication for continued clockwise rotation of the South China block. Geological Society of America Bulletin, 117(3-4): 396-410.

Monié, P., Agard, P., 2009. Coeval blueschist exhumation along thousands of kilometers: Implications for subduction channel processes, Geochem. Geophys. Geosyst., 10, Q07002, doi:10.1029/2009GC002428.

Qiu, L., Yan, D.-P., Yang, W.-X., Wang, J., Tang, X. and Ariser, S., 2017. Early to Middle Triassic sedimentary records in the Youjiang Basin, South China: Implications for Indosinian orogenesis. Journal of Asian Earth Sciences, 141: 125-139.

Ratschbacher, L., Hacker, B.R., Webb, L.E., McWilliams, M., Ireland, T., Dong, S., Calvert, A., Chateigner, D., Wenk, H.R., 2000. Exhumation of the

ultrahigh-pressure continental crust in east central China: Cretaceous and Cenozoic unroofing and the Tan-Lu fault. Journal of Geophysical Research-Solid Earth 105, 13303-13338.

Ratschbacher, L., Hacker, B.R., Calvert, A., Webb, L.E., Grimmer, J.C., McWilliams, M.O., Ireland, T., Dong, S.W., Hu, J.M., 2003. Tectonics of the Qinling (Central China): tectonostratigraphy, geochronology, and deformation history. Tectonophysics 366, 1-53.

Reiners, P. W., Farley, K. A., & Hickes, H. J. (2002). He diffusion and (U-Th)/He thermochronometry of zircon: Initial results from Fish Canyon Tuff and Gold Butte. Tectonophysics, 349, 297–308. https://doi.org/10.1016/S0040-1951(02)00058-6

Reiners, P.W., 2005. Zircon (U-Th)/He thermochronometry. Low-Temperature Thermochronology: Techniques, Interpretations, and Applications 58, 151-179.

Reiners, P. W., Nicolescu, S., 2006. Measurement of parent nuclides for (U-Th)/He chronometry by solution sector ICP-MS. ARHDL Rep. 1 (http://www.geo.arizona.edu/~reiners/arhdl/arhdl.htm).

Roger, F., Leloup, P.H., Jolivet, M., Lacassin, R., Trinh, P.T., Brunel, M., Seward, D., 2000. Long and complex thermal history of the Song Chay metamorphic dome (Northern Vietnam) by multi-system geochronology. Tectonophysics 321, 449-466.

Roger, F., Jolivet, M., Malavieille, J., 2010. The tectonic evolution of the Songpan-Garze(North Tibet) and adjacent areas from Proterozoic to Present: A

synthesis. J Asian Earth Sci 39, 254-269.

Scott, E., Allen, M.B., Macpherson, C.G., McCaffrey, K.J.W., Davidson, J.P., Saville, C., Ducea, M.N., 2018. Andean surface uplift constrained by radiogenic isotopes of arc lavas. Nature Communications 9, doi:10.1038/s41467-018-03173-4.

Shi, W., Wang, F., Yang, L., Wu, L., Zhang, W., 2018. Diachronous growth of the Altyn Tagh Mountains: Constraints on propagation of the northern Tibetan margin from (U-Th)/He dating. Journal of Geophysical Research: Solid Earth, 123, 6000–6018. https://doi.org/10.1029/2017JB014844.

Shu, L.S., Zhou, X.M., Deng, P., Wang, B., Jiang, S.Y., Yu, J.H., Zhao, X.X., 2009. Mesozoic tectonic evolution of the Southeast China Block: New insights from basin analysis. J Asian Earth Sci 34, 376-391.

Shu, L. S., Jahn, B. M., Charvet, J., Santosh, M., Wang, B., Xu, X. S., Jiang, S. Y., 2014. Intraplate tectono-magmatism in the Cathaysia Block (South China): Evidence from stratigraphic, structural, geochemical and geochronological investigations. Am. J. Sci. 314, 154–186.

Shu, L. S., Wang, B., Cawood, P. A., Santosh, M., Xu, Z. Q., 2015. Early Paleozoic and Early Mesozoic intraplate tectonic and magmatic events in the Cathaysia Block, South China. Tectonics 34, 1600–1621.

Strecker, M. R., R. N. Alonso, B. Bookhagen, B. Carrapa, G. E. Hilley, E. R. Sobel, and M. H. Trauth (2007), Tectonics and climate of the southern central Andes, Annual Review of Earth and Planetary Sciences 35, 747-787.

Taghizadeh-Farahmand, F., Afsari, N., Sodoudi, F., 2015. Crustal thickness of Iran inferred from converted waves, Pure Appl. Geophys. 172, 309-331.

Tang, S.-L., Yan, D.-P., Qiu, L., Gao, J.-F. and Wang, C.-L., 2014. Partitioning of the Cretaceous Pan-Yangtze Basin in the central South China Block by exhumation of the Xuefeng Mountains during a transition from extensional to compressional tectonics? Gondwana Research, 25(4): 1644-1659.

Wan, Y., Liu, D., Wilde, S.A., Cao, J., Chen, B., Dong, C., Song, B., Du, L., 2010. Evolution of the Yunkai Terrane, South China: Evidence from SHRIMP zircon U-Pb dating, geochemistry and Nd isotope. J Asian Earth Sci 37, 140-153.

Wang, C., Zhao, X., Liu, Z., Lippert, P.C., Graham, S.A., Coe, R.S., Yi, H., Zhu, L., Liu, S. and Li, Y., 2008. Constraints on the early uplift history of the Tibetan Plateau. Proceedings of the National Academy of Sciences, 105(13): 4987-4992.

Wang, F., Wang, Q., Lin, W., Wu, L., Shi, W., Feng, H., Zhu, R., 2014. 40Ar/39Ar geochronology of the North China and Yangtze Cratons: New constraints on Mesozoic cooling and cratonic destruction under East Asia. Journal of Geophysical Research: Solid Earth, doi: 10.1002/2013jb010708.

Wang, J.-G., Hu, X., Garzanti, E., Ji, W.-Q., Liu, Z.-C., Liu, X.-C., Wu, F.-Y., 2017. Early cretaceous topographic growth of the Lhasaplano, Tibetan plateau: Constraints from the Damxung conglomerate. Journal of Geophysical Research: Solid Earth 122, 5748-5765.Wang, W., Zhou, M.F., Yan, D.P., Li, L., John, M., 2013. Detrital zircon record of Neoproterozoic active-margin sedimentation in the eastern Jiangnan Orogen, South China. Precambrian Res. 235, 1-19.

Wang, W., Zhou, M.-F., Zhao, J.-H., Pandit, M., Zheng, J.-P., Liu, Z.-R., 2016. Neoproterozoic active continental margin in the southeastern Yangtze Block of South China: evidence from the ca. 830-810 Ma sedimentary strata. Sediment. Geol. 342, 254-267.

Wang, X.L., Zhou, J.C., Qiu, J.S., Zhang, W.L., Liu, X.M., Zhang, G.L., 2006. LA-ICP-MS U–Pb zircon geochronology of the Neoproterozoic igneous rocks from Northern Guangxi, South China: implications for tectonic evolution. Precambrian Res. 145, 111–130.

Wang, Y.J., Zhang, Y.H., Fan, W.M., Peng, T.P., 2005. Structural signatures and Ar-40/Ar-39 geochronology of the Indosinian Xuefengshan tectonic belt, South China Block. J Struct Geol 27, 985-998.

Wang, Y.J., Fan, W.M., Cawood, P.A., Ji, S.C., Peng, T.P., Chen, X.Y., 2007. Indosinian high-strain deformation for the Yunkaidashan tectonic belt, south China: Kinematics and Ar-40/Ar-39 geochronological constraints. Tectonics 26.

Webb, L.E., Hacker, B.R., Ratschbacher, L., McWilliams, M.O., Dong, S., 1999. Thermochronologic constraints on deformation and cooling history of high- and ultrahigh-pressure rocks in the Qinling-Dabie orogen, eastern China. Tectonics 18, 621-638.

Wei, W., Chen, Y., Faure, M., Martelet, G., Lin, W., Wang, Q., Yan, Q., Hou, Q., 2016. An early extensional event of the South China Block during the Late Mesozoic recorded by the emplacement of the Late Jurassic syntectonic Hengshan Composite Granitic Massif (Hunan, SE China). Tectonophysics 672–673, 50-67.

Wolf, R. A., Farley, K. A., Silver, L. T., 1996. Helium diffusion and low-temperature thermochronometry of apatite. Geochimica et Cosmochimica Acta, 60, 4231–4240. https://doi.org/10.1016/S0016-7037(96)00192-5.

Wu, L., Monié, P., Wang, F., Lin, W., Ji, W., Bonno, M., 2016. Cenozoic exhumation history of Sulu terrane: Implications from (U–Th)/He thermochronology. Tectonophysics, 672–673, 1–15. https://doi.org/10.1016/j.tecto.2016.01.035

Wu, F.-Y., Yang, J.-H., Xu, Y.-g., Wilde, S.A., Walker, R.J., 2019. Destruction of the North China Craton in the Mesozoic. Annual Review of Earth and Planetary Sciences, 47, 173-195.

Xu, G., Wang, E., 2010. The uplift mechanism of Tongbai complex in Mesozoic and its coupling relationship with Nanyang Basin. Chinese Journal of Geology, 45(3), 626-652 (in Chinese with English abstract).

Xu, X.B., Zhang, Y.Q., Shu, L.S., Jia, D., 2011. La-ICP-MS U-Pb and 40Ar/39Ar geochronology of the sheared metamorphic rocks in the Wuyishan: Constraints on the timing of Early Paleozoic and Early Mesozoic tectono-thermal events in SE China. Tectonophysics 501, 71-86.

Xue, Z., Martelet, G., Lin, W., Faure, M., Chen, Y., Wei, W., Li, S., Wang, Q., 2017. Mesozoic Crustal Thickening of the Longmenshan Belt (NE Tibet, China) by Imbrication of Basement Slices: Insights from Structural Analysis, Petrofabric and Magnetic Fabric Studies, and Gravity Modeling. Tectonics 36, 3110-3134.

Yan, D.P., Zhou, M.F., Song, H.L., Wang, X.W., Malpas, J., 2003. Origin and tectonic significance of a Mesozoic multi-layer over-thrust system within the Yangtze

Block (South China). Tectonophysics 361, 239-254.

Yan, D.P., Zhou, M.F., Li, S.B., Wei, G.Q., 2011. Structural and geochronological constraints on the Mesozoic-Cenozoic tectonic evolution of the Longmen Shan thrust belt, eastern Tibetan Plateau. Tectonics 30, TC6005, doi:10.1029/2011TC002867.

Yang, D.-S., Li, X.-H., Li, W.-X., Liang, X.-Q., Long, W.-G., Xiong, X.-L., 2010. U-Pb and 40Ar-39Ar geochronology of the Baiyunshan gneiss (central Guangdong, south China): constraints on the timing of early Palaeozoic and Mesozoic tectonothermal events in the Wuyun (Wuyi-Yunkai) Orogen. Geol Mag 147, 481-496.

Yin, A., and Nie, S., 1996, A Phanerozoic palinspastic reconstruction of China and its neighboring regions, in The Tectonic Evolution of Asia edited by A. Yin and T.M. Harrison, Cambridge University Press, p. 442-485.

Yonkee, W.A., Weil, A.B., 2015. Tectonic evolution of the Sevier and Laramide belts within the North American Cordillera orogenic system. Earth-Science Reviews 150, 531-593.

Zhang, Q., Wang, Y.L., Jin, W.J., Li, C.D., 2008. Eastern China Plateau during the Late Mesozoic: evidence, problems and implication. Geological Bulletin of China, 27(9):1404-1430 (in Chinese with English abstract).

Zhang, J., Ma, Z.J., Yang, J., Chen, B.H., Lei, Y.L., Wang, Z.X., Li, T., 2010. The attributes of the Mesozoic basins along the western foothill of the Xuefengshan Mountains and its tectonic implications. Acta Geol Sin 84(5), 631-650 (in

Chinese with English abstract).

Zheng, Y.F., Gong, B., Zhao, Z.F., Wu, Y.B., Chen, F.K., 2008. Zircon U-Pb age and O isotope evidence for Neoproterozoic low-O-18 magmatism during supercontinental rifting in South China: Implications for the snowball Earth event. Am J Sci 308, 484-516.

Zhong, D., 2000. Paleotethysides in West Yunnan and Sichuan, China.Science Press, Beijing, 248 p.

Zhou, X.M., Li, W.X., 2000. Origin of Late Mesozoic igneous rocks in Southeastern China: implications for lithosphere subduction and underplating of mafic magmas. Tectonophysics 326, 269-287.

Zhou, X.M., Sun, T., Shen, W.Z., Shu, L.S., Niu, Y.L., 2006. Petrogenesis of Mesozoic granitoids and volcanic rocks in South China: A response to tectonic evolution. Episodes 29, 26-33.

Zhu, G., Xie, C.-L., Chen, Y., Xiang, B.-W., Hu, Z.-Q., 2010. Evolution of the Hongzhen metamorphic core complex: Evidence for Early Cretaceous extension in the eastern Yangtze craton, eastern China. Geol Soc Am Bull 122, 506-516.

Figure captions

Fig. 1. Tectonic map of the South China Block and its adjacent regions. CB: Cathaysia Block. ICB: Indochina Block. JSJ: Jinshajiang Suture zone. NCB: North China Block. SCB: South China Block. XFS: Xuefengshan. YB: Yangtze Block. DEM base map is generated from the software GeoMapApp (http://www.geomapapp.org). Metamorphic

units of Triassic orogens are highlighted in pink.

Fig.2. Geological map of the Xuefengshan Belt (Modified after Chu et al., 2012a). BP: Baimashan pluton. EZ: Eastern Zone. HS: Hengshan. MP: Miaoershan pluton. MXT: Main Xuefengshan Thrust. WZ: Western Zone. YB: Yuanma Basin. YP: Yuechengling pluton. Sample localities of the north orogenic core and the south orogenic core are marked in Figs. 3a and 5a.

Fig. 3. (a) Geological map of the south orogenic core (SOC). Structural elements including foliation and lineation measurements are based on this study and Chu et al. (2012b). (b) Cross-section showing the Triassic décollement zone overprinted by Cretaceous extension. Note that the interface between the décollement zone and the weakly- or unmetamorphosed sedimentary cover was inherited during the Cretaceous reworking.

Fig. 4. Field photos and photomicrographs of structures observed in the south orogenic core. (a) Crenulated mylonitic foliation in the north of the décollement, location of sample XF295. (b) Folded mylonitic foliation of the décollement zone, location of sample XF300. (c) Quartz micaschist with pervasive crenulation, south of the décollement. (d) Crenulation folding the stretching lineation during the Triassic deformation, location of sample XF316B. (e) Superimposed S_c crenulation in mica-rich layers, but Triassic mylonitic foliation (S_1) preserved in quartz-rich layers.

Location at 500 m west of sample XF365. (f) Strongly crenulated micaschist (S_c) superimposed of S_1 foliation. Note that the wavelength of crenulations is about 0.5-2 mm. Location at sample XF295. (g) Gently crenulated micaschist. Location at sample XF312. (h) Undeformed Miaoershan pluton. Note the points with incipient buldging recrystallization of large quartz grains. Location at sample XF270.

Fig. 5. (a) Geological map of the north orogenic core. Structural elements including foliation and lineation measurements are based on this study and Chu et al. (2012b). (b) Cross-section showing the Triassic décollement zone of the NOC.

Fig. 6. Geological map with sample locations and Ar-Ar and (U-Th)/He ages of samples in this study from the south orogenic core. Symbols for rock units are the same as those in Fig. 2a.

Fig. 7. ^{40}Ar-^{39}Ar mica dating results in the study region. Age spectra are presented for (a) XF270, (b) XF300, (c) XF312, (d) XF313, (e) and (f) XF314, (g) XF316B, and (h) XF224. Sample locations are marked on Figs. 3 and 5. Bt: Biotite. Mus: Muscovite.

Fig. 8. ^{40}Ar-^{39}Ar mica dating results in the Chengbu region. Age spectra are presented for (a) XF295A, (b) and (c) XF365. Sample locations are marked on Fig. 3. Bt: Biotite. Mus: Muscovite.

Fig. 9. ^{40}Ar–^{39}Ar K-feldspar age spectra and the multi-domain diffusion modeling results of K-feldspar from (a) and (b): XF 270, and (c) and (d): XF349. Sample locations are marked on Figs. 3 and 5.

Fig. 10. Cooling paths of (a) the south orogenic core of the XFSB, and (b) the north orogenic core. In the south orogenic core, there were two episodes of fast cooling, whereas only the second episode is recorded in the north orogenic core.

Fig. 11. Summary of available cooling paths related to Cretaceous exhumation of Triassic orogens in East Asia. (a) Marginal belts around the SCB, including Dabieshan, Tongbaishan, and Sulu modified after Li et al. (2015); Song Chay data are from Roger et al. (2000). (b) Intracontinental belts, including Baiyunshan (Yang et al., 2010), Yunkai Massif (Wang et al., 2007a; Chen et al., 2017), and Xuefengshan (this study). See Fig. 1 for locations. Dashed parts of each cooling path represent a presumed thermal trajectory of the belt.

Fig. 12. Tectonic models showing the evolution of the South China Block in the Triassic and Cretaceous within the Paleo-Pacific subduction system. (a) A broad intracontinental belt was created by flat-slab subduction (Li and Li, 2007), producing an orogenic plateau that is similar to the present North American Cordillera, or Andes. The north orogenic core (NOC) of the Triassic belts experienced limited exhumation, whereas the south orogenic core (SOC) showed little effect. Continuous subduction in

Jurassic maintained the plateau without further exhumation. (b) The two-stage Cretaceous extension exhumed the metamorphic orogenic cores of the Triassic belts, and finalized the current geological configuration of the South China Block. This phase of extension marked the collapse of the Mesozoic orogenic plateau in the South China Block.

Fig. 13. Area vs. time for comparison of present and ancient plateaux in major subduction (light color) and collision (dark color) zones. Note that there is a change from subduction to collision for the Lhasaplano. Area is estimated by using Google Earth. Data for duration of plateaux are from: 1. Wang et al. (2008), Law and Allen (2020); 2. Francois et al. (2014); 3. This study; 4. DeCelles (2004); 5. Kapp (2007), Wang et al. (2017); 6. McQuarrie et al. (2008), Scott et al. (2018).

Table 1. Summary of information from dated samples of the Xuefengshan Belt. Weighted age refers to weighted plateau age for Ar-Ar dating, and weighted mean age for (U-Th)/He dating.

Appendix Table S1. Analytical Ar-Ar data of selected samples analyzed in Institute of Geology and Geophysics, Chinese Academy of Sciences.

Appendix Table S2. Analytical Ar-Ar data of selected samples analyzed in Geosciences Montpellier, University of Montpellier.

Appendix Table S3. Analytical data on K-feldspar Ar-Ar dating of two granites.

Appendix Table S4. Analytical data on zircon (U-Th)/He dating from the south orogenic core.

Appendix Table S5. Analytical data on apatite (U-Th)/He dating from the south orogenic core.

A large plateau can be produced by crustal thickening in convergent zones such as continental collision belts and Andean-type subduction zones, but the life cycles of such plateaux are not well-understood. In particular, it is not clear how long they persist after construction, before other tectonic processes or erosion reduce crustal thickness and elevation to near-normal levels. Triassic subduction- and collision-tectonics produced intense deformation, magmatism and metamorphism across the entire South China Block. This large-scale crustal shortening created a broad orogenic belt, uplifted most parts of the South China Block, and probably initiated the growth of an orogenic plateau. Our study presents low-temperature thermochronology data from the Xuefengshan Belt in the interior of the South China Block. There was along-strike variation in exhumation. The north orogenic core was subjected to Triassic (~245-210 Ma), and Late Cretaceous (~100-80 Ma) exhumation, whereas the cooling path of the south orogenic core reflects a two stage Cretaceous evolution. The variable exhumation pattern reflects non-uniform tectonics in different regions, but both regions were subject to Late Cretaceous extension. We tentatively reconstruct the original plateau paleo-elevation to be ~1.5 km above sea level, based on the amount of exhumation (~10 km) and the present crustal thickness (~35 km). The T-t trajectories of the Xuefengshan Belt and other Triassic belts highlight the significance of Cretaceous extension and exhumation in shaping the tectonic configuration of the South China Block. Large-scale extension was probably triggered by rollback of the Paleo-Pacific subduction zone.

Yang Chu: Conceptualization, Methodology, Visualization, Writing - Original Draft, Writing - Review & Editing.
Wei Lin: Investigation, Supervision, Writing - Review & Editing, Funding acquisition
Michel Faure: Investigation, Visualization, Writing - Review & Editing
Mark B. Allen: Methodology, Visualization, Writing - Review & Editing,
Zhentian Feng: Investigation

Declaration of interests

☒ The authors declare that they have no known competing financial interests or personal relationships that could have appeared to influence the work reported in this paper.

☐The authors declare the following financial interests/personal relationships which may be considered as potential competing interests:

Highlights:

1. Thermochronology defines T-t cooling paths for the Xuefengshan Belt, South China

2. Orogenic cores of this Triassic belt were mainly exhumed to surface in Cretaceous

3. Episodic Cretaceous extension and exhumation finalized the tectonic configuration

4. A regional Mesozoic orogenic plateau was dissected by Cretaceous extension

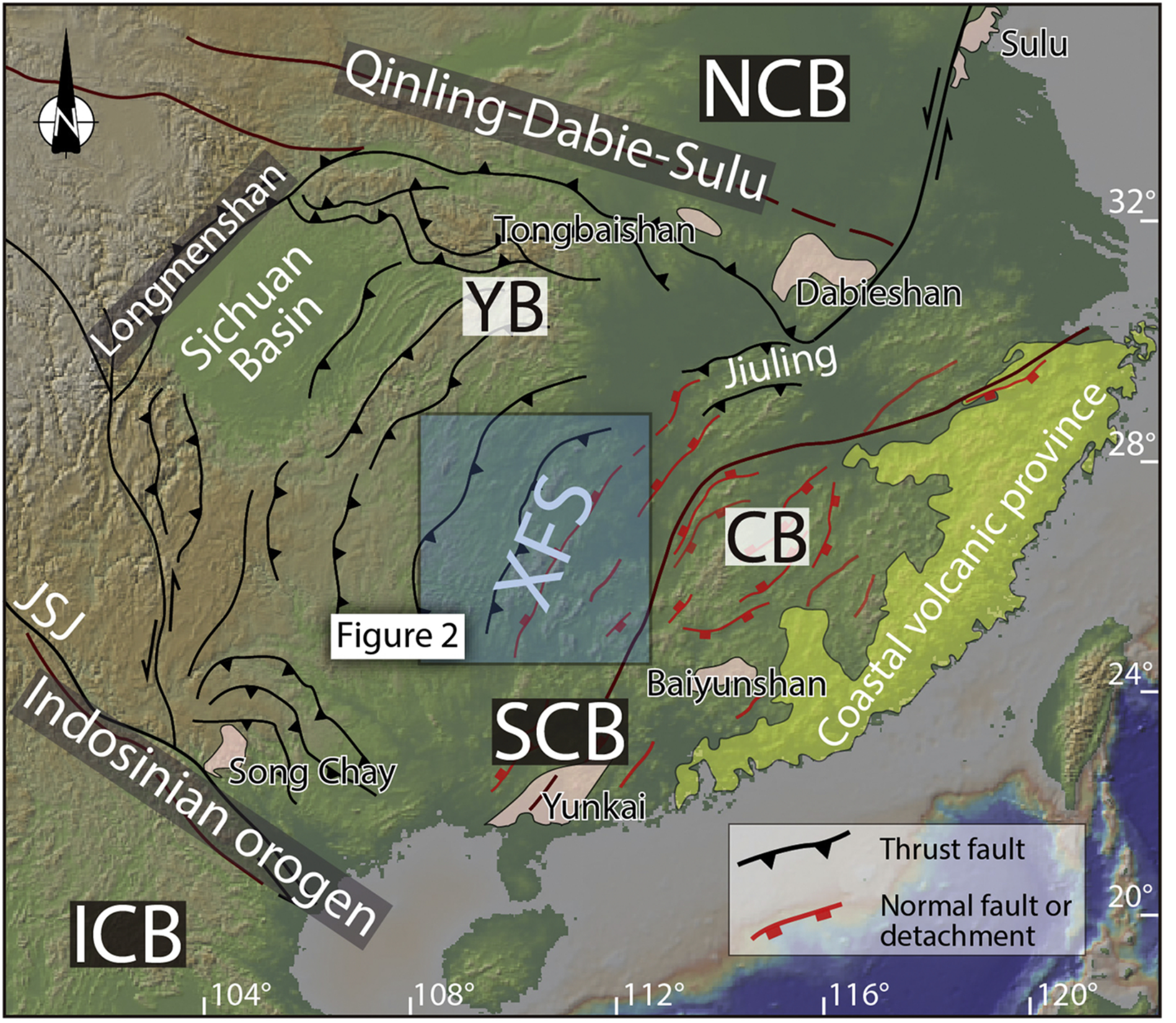
Sulu
NCB
Qinling-Dabie-Sulu
Longmenshan
Sichuan Basin
Tongbaishan
YB
Dabieshan
Jiuling
32°
28°
XFS
CB
Coastal volcanic province
Figure 2
JSJ
Indosinian orogen
Baiyunshan
24°
SCB
Song Chay
Yunkai
Thrust fault
Normal fault or detachment
20°
ICB
104°
108°
112°
116°
120°

Figure 1

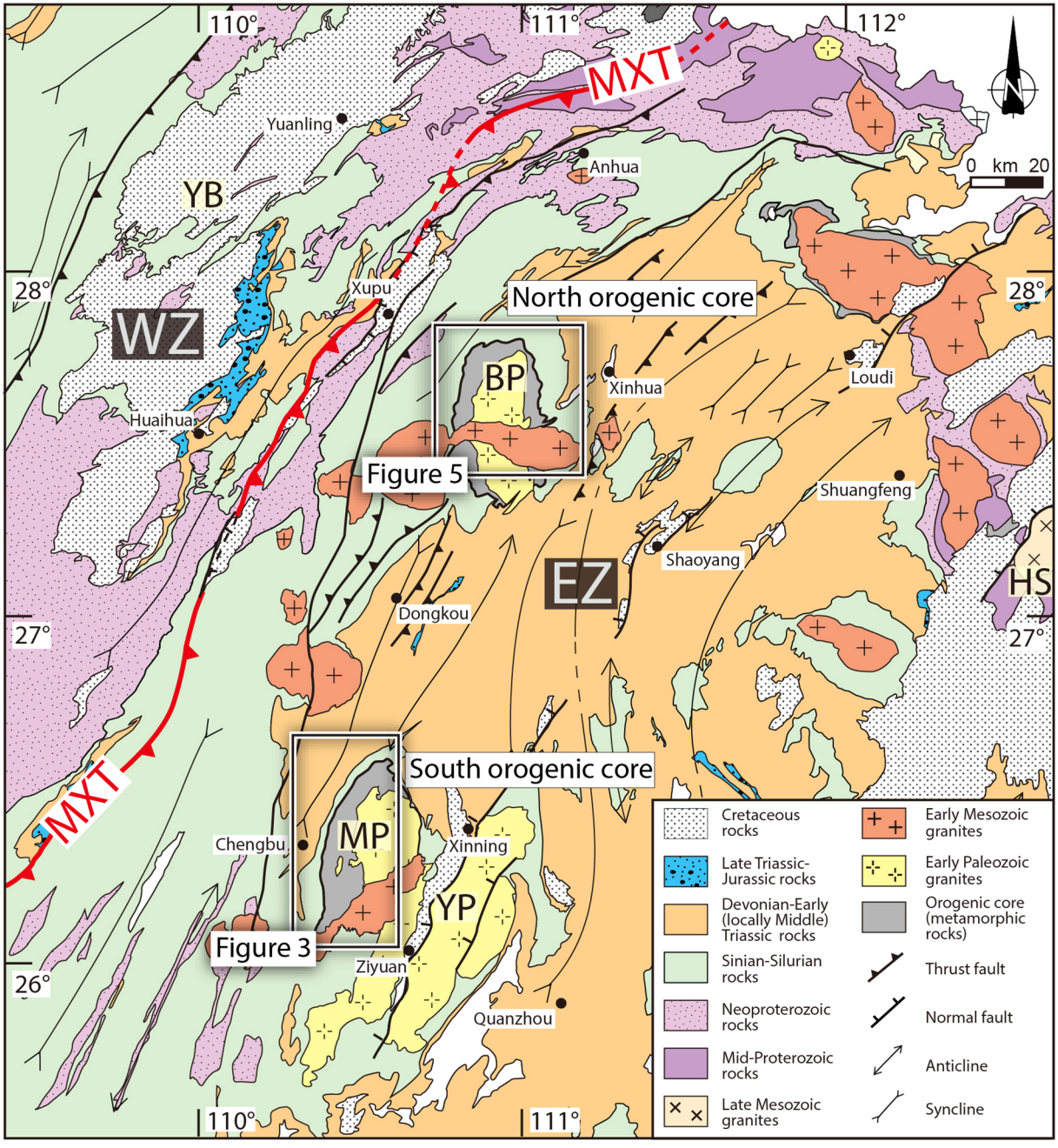
110°
111°
112°
MXT
Yuanling
Anhua
YB
0 km 20
28°
Xupu
North orogenic core
WZ
BP
Xinhua
Loudi
Huaihua
Figure 5
Shuangfeng
Shaoyang
EZ
HS
Dongkou
27°
South orogenic core
MXT
Chengbu
MP
Xinning
YP
Figure 3
Ziyuan
26°
Quanzhou
Cretaceous rocks
Late Triassic-Jurassic rocks
Devonian-Early (locally Middle) Triassic rocks
Sinian-Silurian rocks
Neoproterozoic rocks
Mid-Proterozoic rocks
Late Mesozoic granites
Early Mesozoic granites
Early Paleozoic granites
Orogenic core (metamorphic rocks)
Thrust fault
Normal fault
Anticline
Syncline

Figure 2

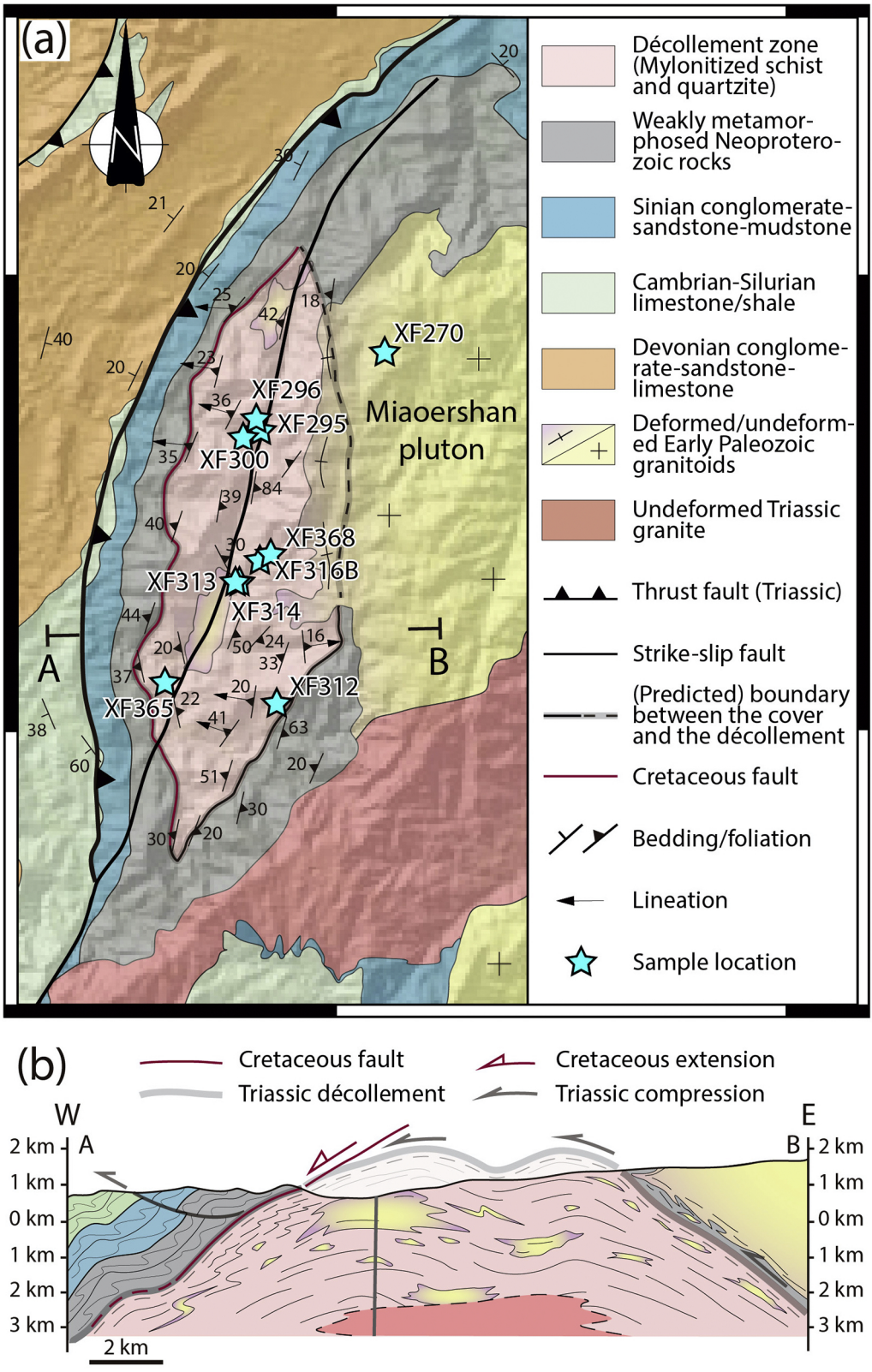
110°30′E
110°45′E
26°30′N
26°15′N
(a)
Décollement zone (Mylonitized schist and quartzite)
Weakly metamorphosed Neoproterozoic rocks
Sinian conglomerate-sandstone-mudstone
Cambrian-Silurian limestone/shale
Devonian conglomerate-sandstone-limestone
Deformed/undeformed Early Paleozoic granitoids
Undeformed Triassic granite
Thrust fault (Triassic)
Strike-slip fault
(Predicted) boundary between the cover and the décollement
Cretaceous fault
Bedding/foliation
Lineation
Sample location
Miaoershan pluton
XF270
XF296
XF295
XF300
XF368
XF316B
XF313
XF314
XF312
XF365
A
B
(b)
Cretaceous fault
Triassic décollement
Cretaceous extension
Triassic compression
W
E
2 km
1 km
0 km
1 km
2 km
3 km
2 km

Figure 3

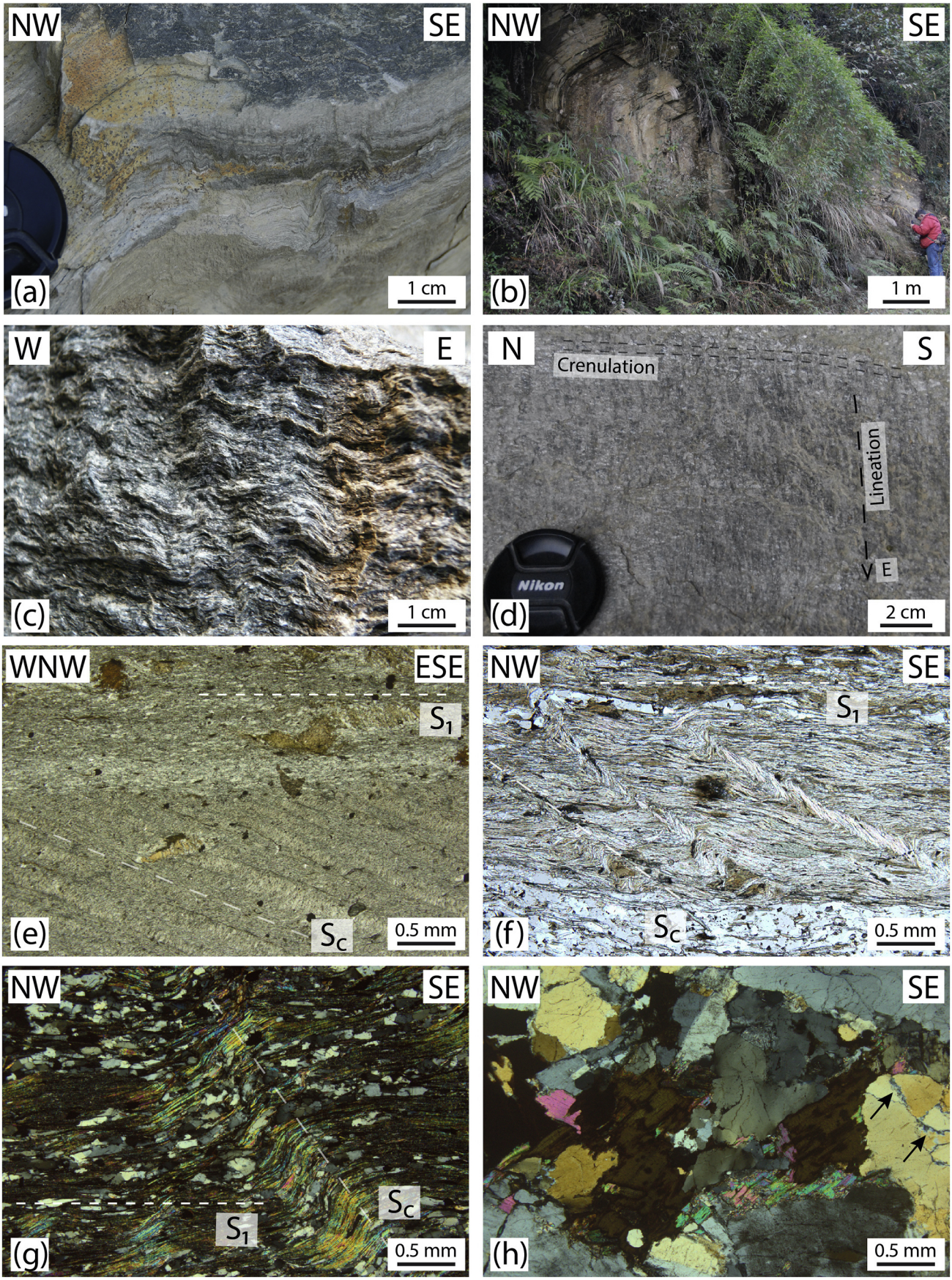
NW
SE
(a)
1 cm
NW
SE
(b)
1 m
W
E
(c)
1 cm
N
S
Crenulation
Lineation
V E
Nikon
(d)
2 cm
WNW
ESE
S_1
(e)
S_C
0.5 mm
NW
SE
S_1
(f)
S_C
0.5 mm
NW
SE
S_C
S_1
(g)
0.5 mm
NW
SE
(h)
0.5 mm

Figure 4

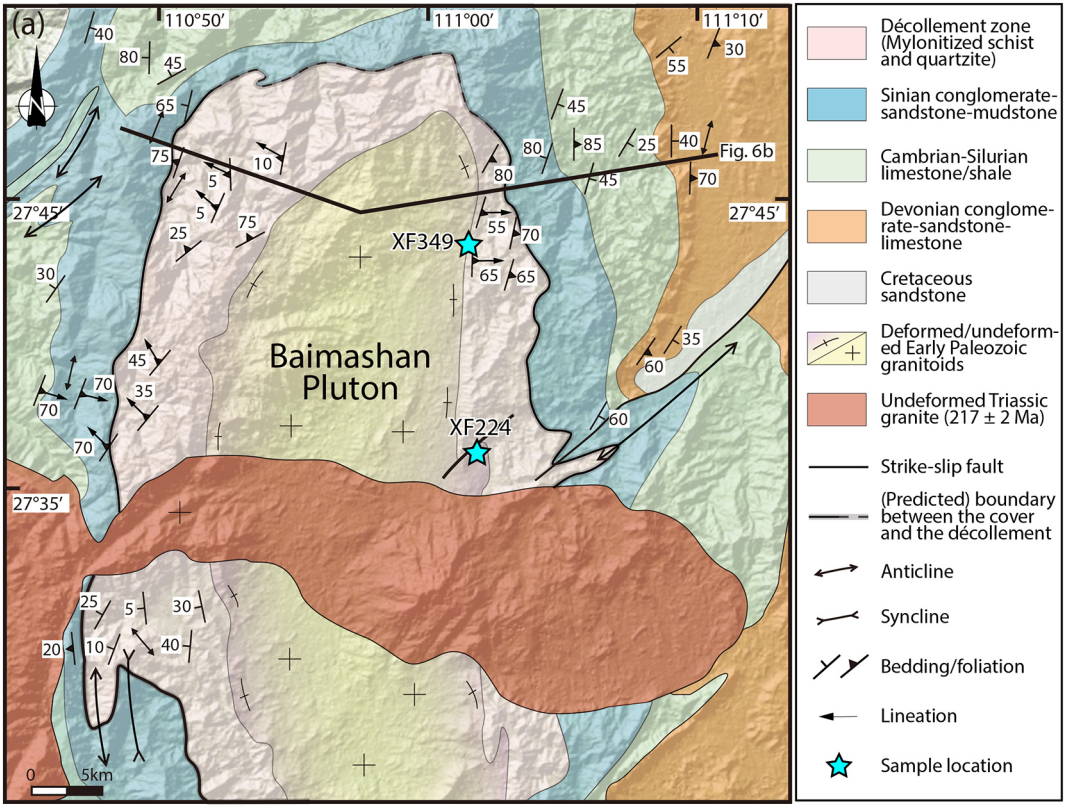
(a)
110°50′
111°00′
111°10′
27°45′
27°35′
Fig. 6b
XF349
XF224
Baimashan Pluton
0
5km
Décollement zone (Mylonitized schist and quartzite)
Sinian conglomerate-sandstone-mudstone
Cambrian-Silurian limestone/shale
Devonian conglomerate-sandstone-limestone
Cretaceous sandstone
Deformed/undeformed Early Paleozoic granitoids
Undeformed Triassic granite (217 ± 2 Ma)
Strike-slip fault
(Predicted) boundary between the cover and the décollement
Anticline
Syncline
Bedding/foliation
Lineation
Sample location

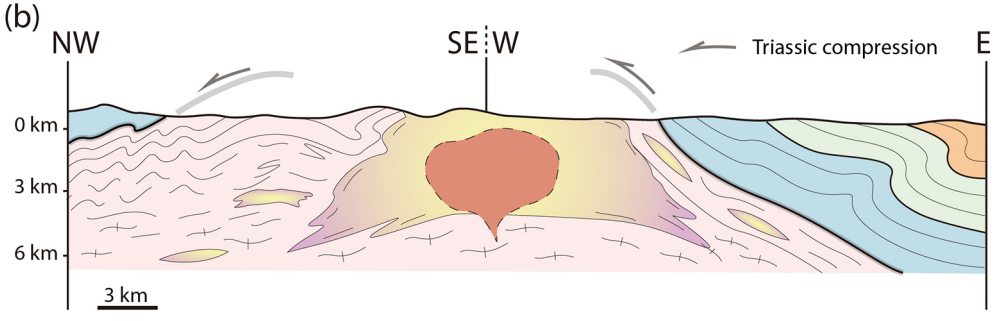
(b)
NW
SE
W
E
Triassic compression
0 km
3 km
6 km
3 km

Figure 5

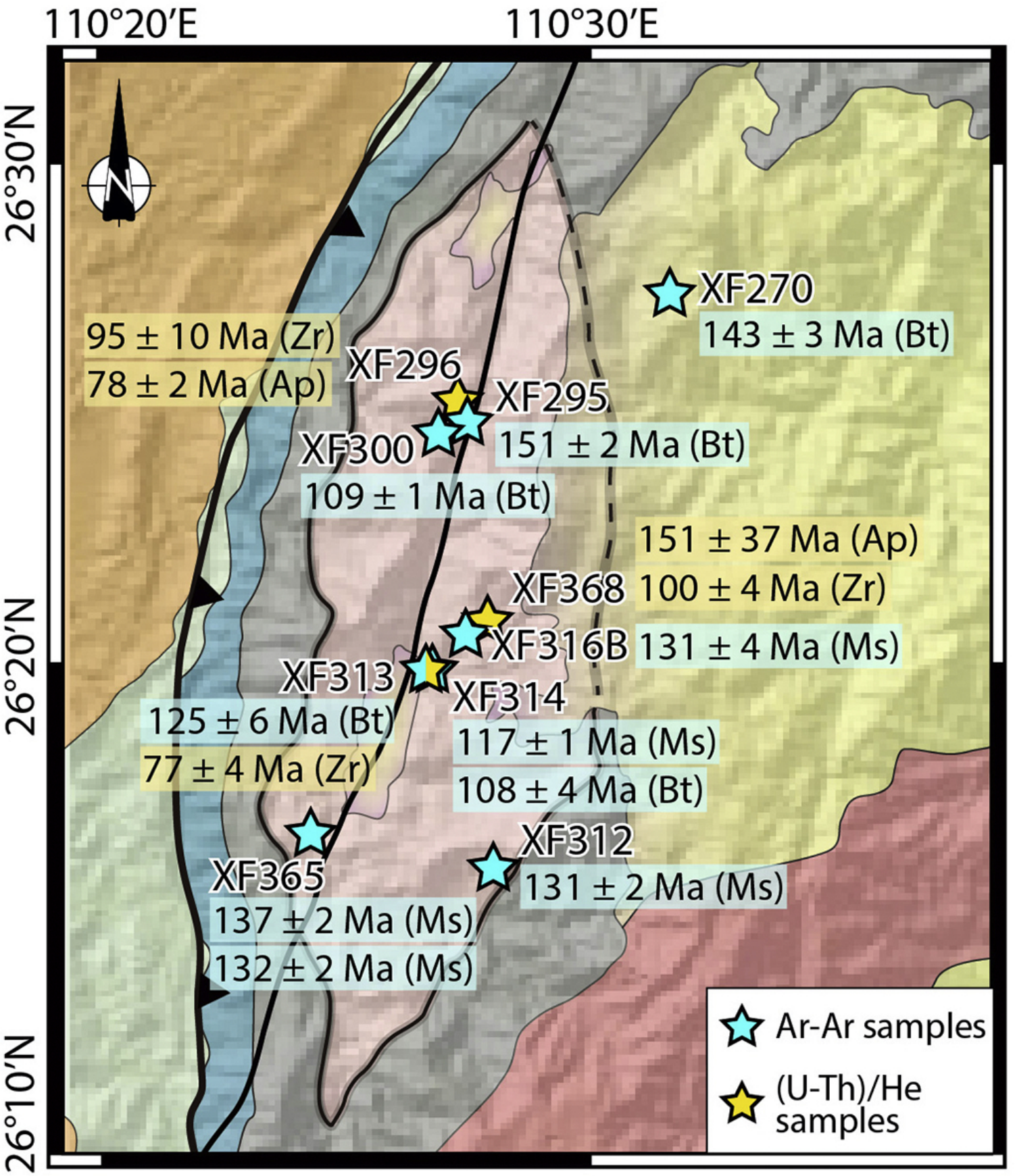
110°20′E
110°30′E
26°30′N
26°20′N
26°10′N
N
XF270
143 ± 3 Ma (Bt)
95 ± 10 Ma (Zr)
78 ± 2 Ma (Ap)
XF296
XF295
XF300
151 ± 2 Ma (Bt)
109 ± 1 Ma (Bt)
151 ± 37 Ma (Ap)
XF368
100 ± 4 Ma (Zr)
XF316B
131 ± 4 Ma (Ms)
XF313
XF314
125 ± 6 Ma (Bt)
77 ± 4 Ma (Zr)
117 ± 1 Ma (Ms)
108 ± 4 Ma (Bt)
XF312
131 ± 2 Ma (Ms)
XF365
137 ± 2 Ma (Ms)
132 ± 2 Ma (Ms)
Ar-Ar samples
(U-Th)/He samples

Figure 6

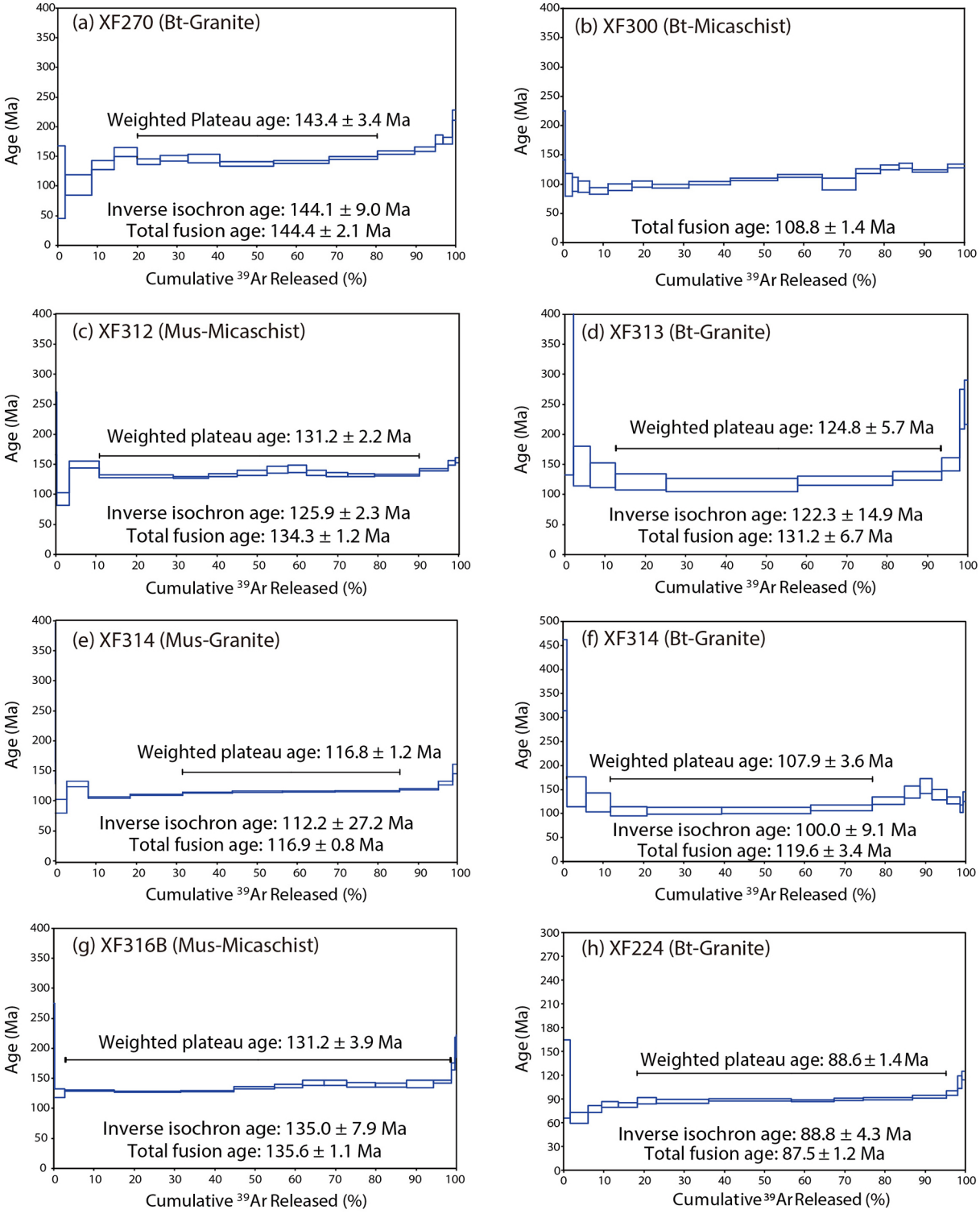
(a) XF270 (Bt-Granite)
Weighted Plateau age: 143.4 ± 3.4 Ma
Inverse isochron age: 144.1 ± 9.0 Ma
Total fusion age: 144.4 ± 2.1 Ma
(b) XF300 (Bt-Micaschist)
Total fusion age: 108.8 ± 1.4 Ma
(c) XF312 (Mus-Micaschist)
Weighted plateau age: 131.2 ± 2.2 Ma
Inverse isochron age: 125.9 ± 2.3 Ma
Total fusion age: 134.3 ± 1.2 Ma
(d) XF313 (Bt-Granite)
Weighted plateau age: 124.8 ± 5.7 Ma
Inverse isochron age: 122.3 ± 14.9 Ma
Total fusion age: 131.2 ± 6.7 Ma
(e) XF314 (Mus-Granite)
Weighted plateau age: 116.8 ± 1.2 Ma
Inverse isochron age: 112.2 ± 27.2 Ma
Total fusion age: 116.9 ± 0.8 Ma
(f) XF314 (Bt-Granite)
Weighted plateau age: 107.9 ± 3.6 Ma
Inverse isochron age: 100.0 ± 9.1 Ma
Total fusion age: 119.6 ± 3.4 Ma
(g) XF316B (Mus-Micaschist)
Weighted plateau age: 131.2 ± 3.9 Ma
Inverse isochron age: 135.0 ± 7.9 Ma
Total fusion age: 135.6 ± 1.1 Ma
(h) XF224 (Bt-Granite)
Weighted plateau age: 88.6 ± 1.4 Ma
Inverse isochron age: 88.8 ± 4.3 Ma
Total fusion age: 87.5 ± 1.2 Ma
Age (Ma)
Cumulative ^{39}Ar Released (%)

Figure 7

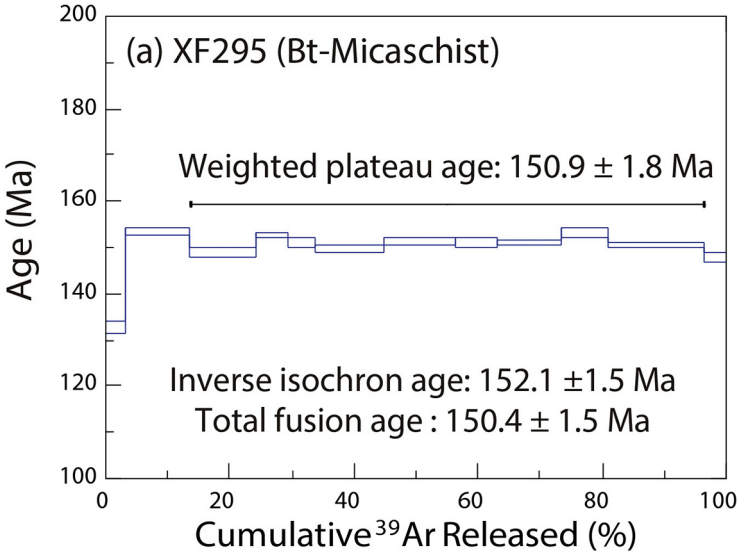
(a) XF295 (Bt-Micaschist)
Weighted plateau age: 150.9 ± 1.8 Ma
Inverse isochron age: 152.1 ±1.5 Ma
Total fusion age : 150.4 ± 1.5 Ma
Age (Ma)
Cumulative ^{39}Ar Released (%)

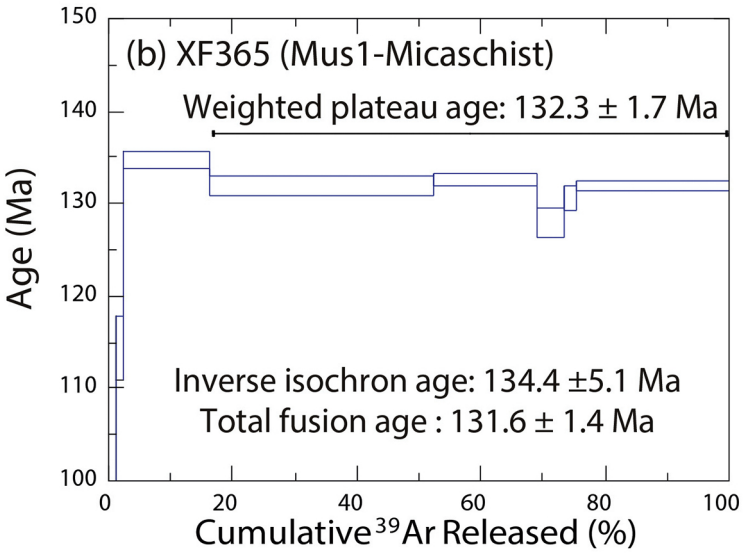
(b) XF365 (Mus1-Micaschist)
Weighted plateau age: 132.3 ± 1.7 Ma
Inverse isochron age: 134.4 ±5.1 Ma
Total fusion age : 131.6 ± 1.4 Ma
Age (Ma)
Cumulative ^{39}Ar Released (%)

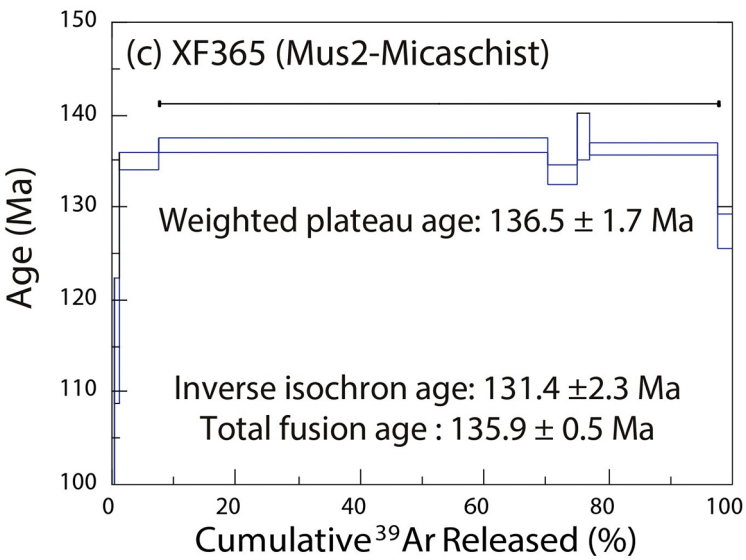
(c) XF365 (Mus2-Micaschist)
Weighted plateau age: 136.5 ± 1.7 Ma
Inverse isochron age: 131.4 ±2.3 Ma
Total fusion age : 135.9 ± 0.5 Ma
Age (Ma)
Cumulative ^{39}Ar Released (%)

Figure 8

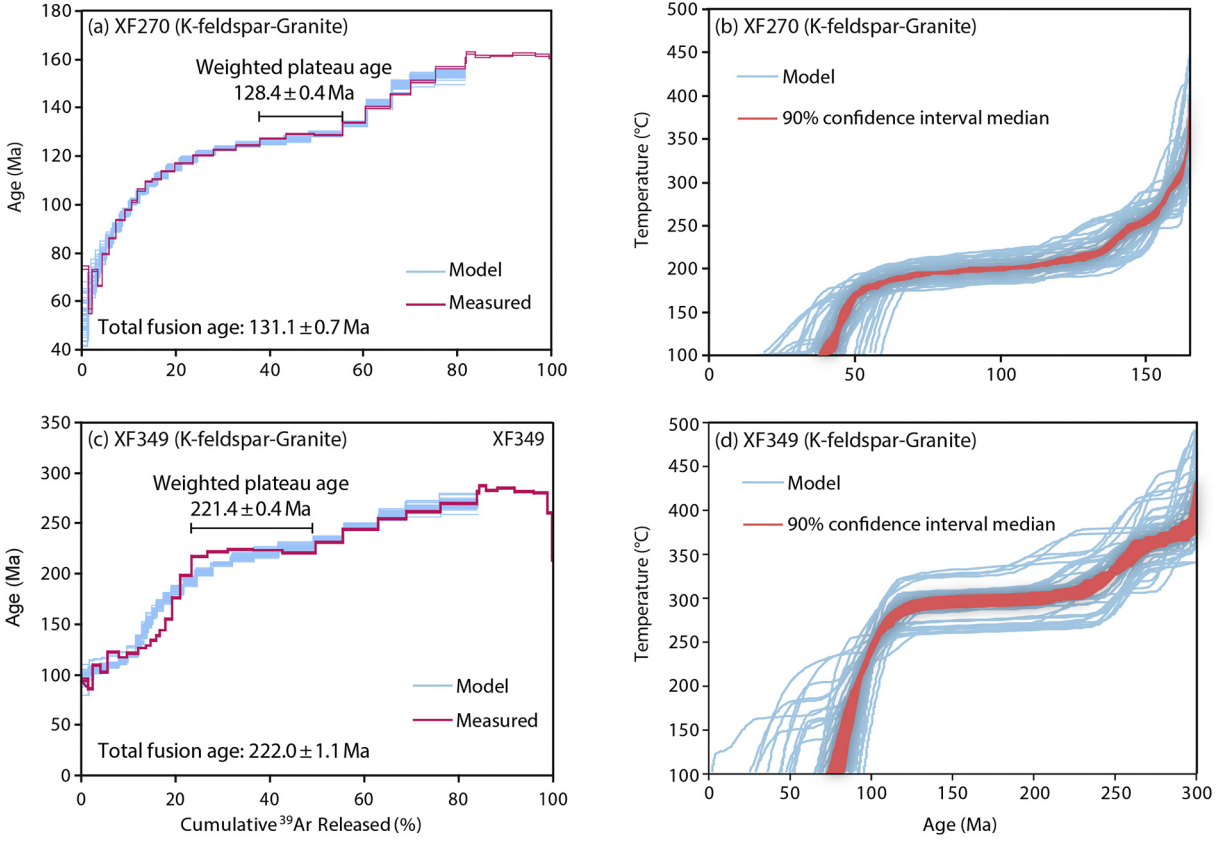
(a) XF270 (K-feldspar-Granite)
Weighted plateau age
128.4 ± 0.4 Ma
Model
Measured
Total fusion age: 131.1 ± 0.7 Ma
Age (Ma)
(b) XF270 (K-feldspar-Granite)
Model
90% confidence interval median
Temperature (°C)
(c) XF349 (K-feldspar-Granite)
XF349
Weighted plateau age
221.4 ± 0.4 Ma
Model
Measured
Total fusion age: 222.0 ± 1.1 Ma
Age (Ma)
Cumulative ^{39}Ar Released (%)
(d) XF349 (K-feldspar-Granite)
Model
90% confidence interval median
Temperature (°C)
Age (Ma)

Figure 9

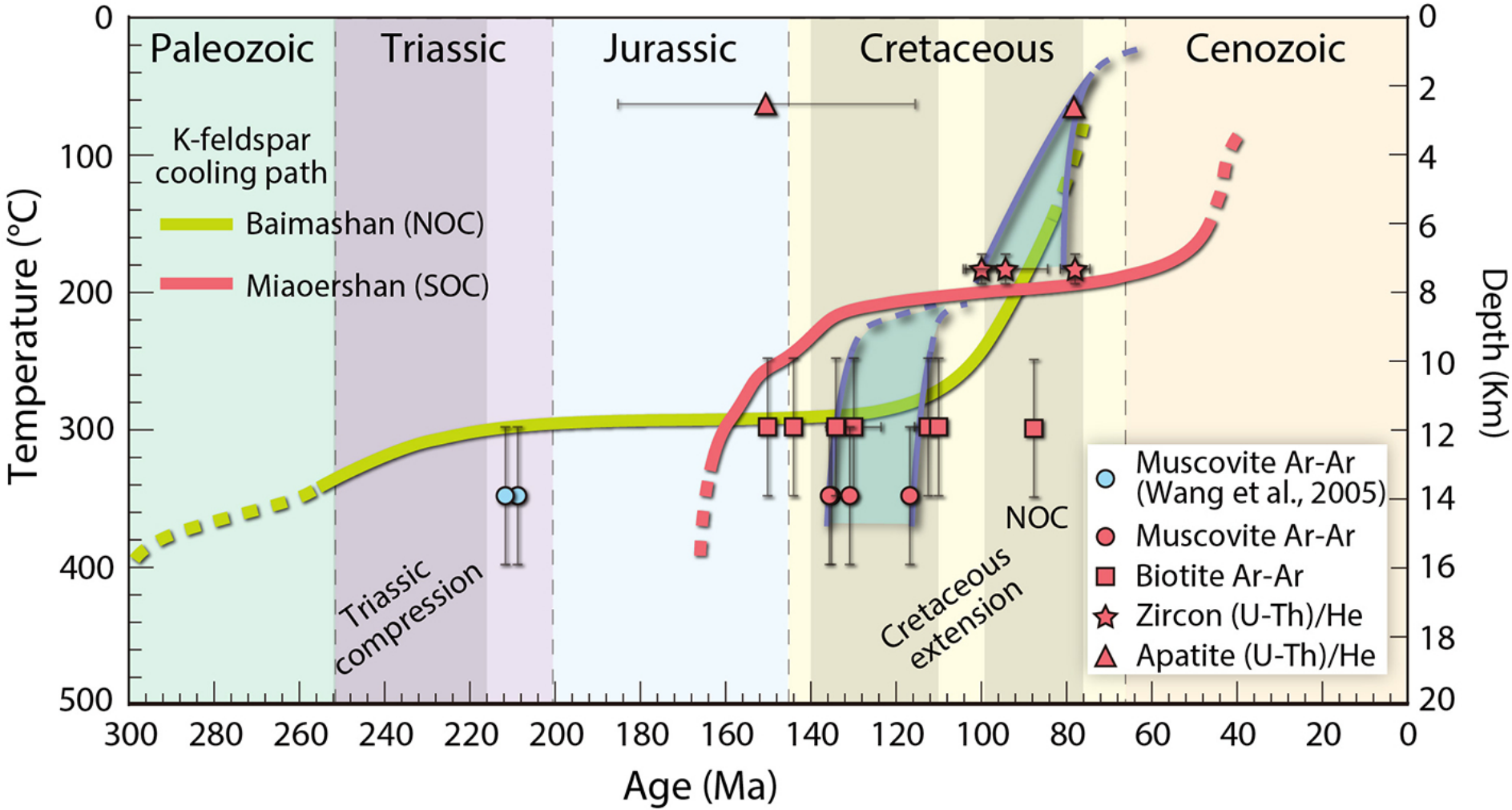
Paleozoic
Triassic
Jurassic
Cretaceous
Cenozoic
K-feldspar cooling path
Baimashan (NOC)
Miaoershan (SOC)
Triassic compression
Cretaceous extension
NOC
Muscovite Ar-Ar (Wang et al., 2005)
Muscovite Ar-Ar
Biotite Ar-Ar
Zircon (U-Th)/He
Apatite (U-Th)/He
Temperature (°C)
Depth (Km)
Age (Ma)
0
100
200
300
400
500
0
2
4
6
8
10
12
14
16
18
20
300
280
260
240
220
200
180
160
140
120
100
80
60
40
20
0

Figure 10

(a) Marginal belts

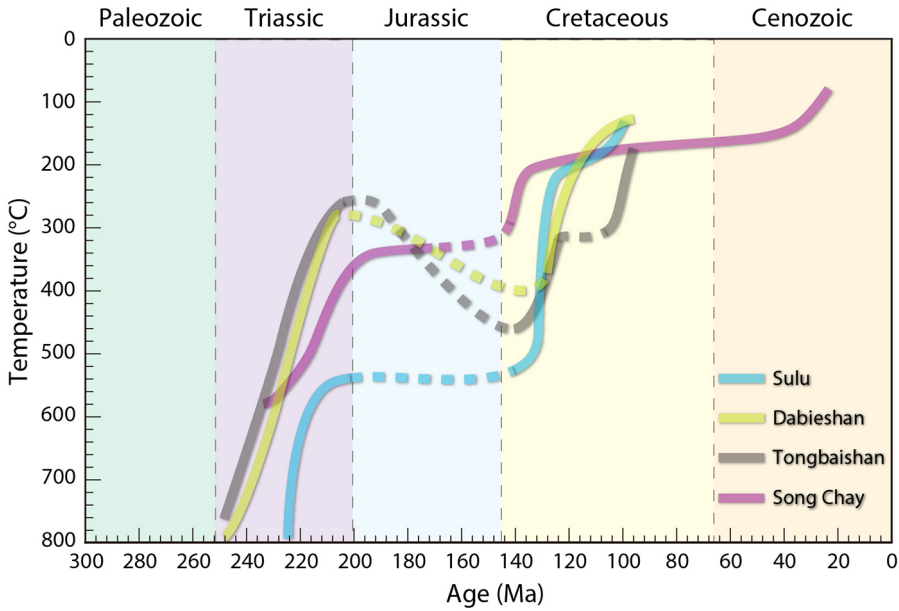

(b) Intracontinental belts

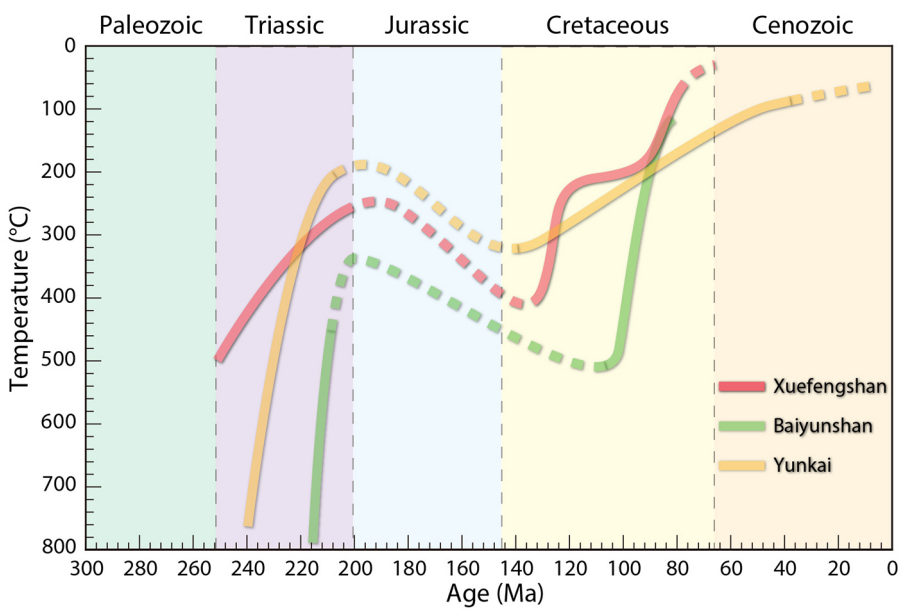

Figure 11

(a) Triassic: Flat subduction and formation of an orogenic plateau

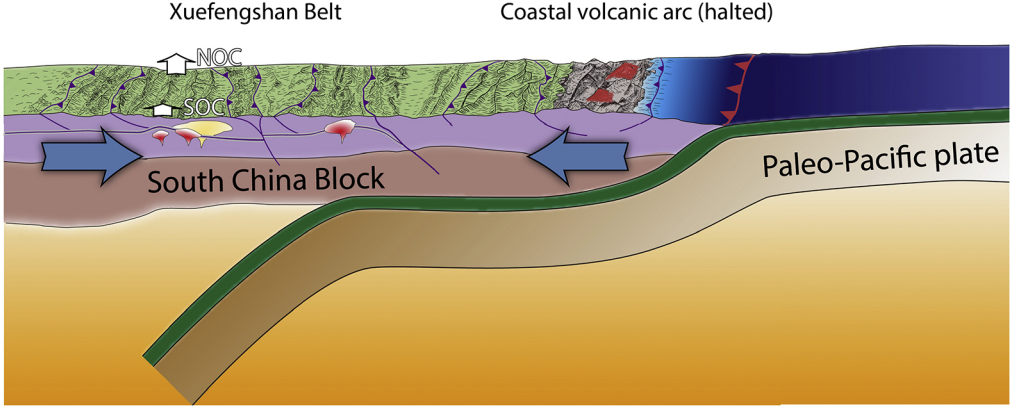

(b) Cretaceous: Back-arc extension and dissection of the plateau

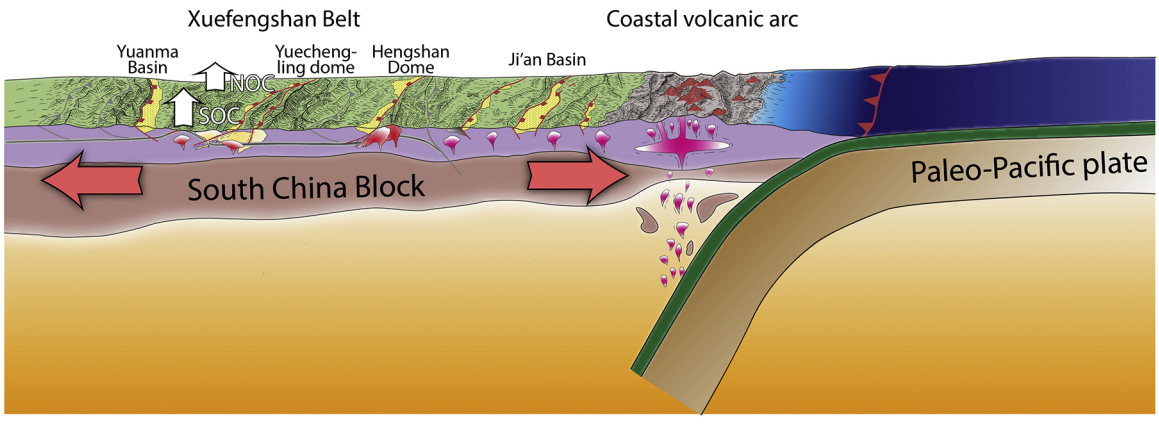

Figure 12

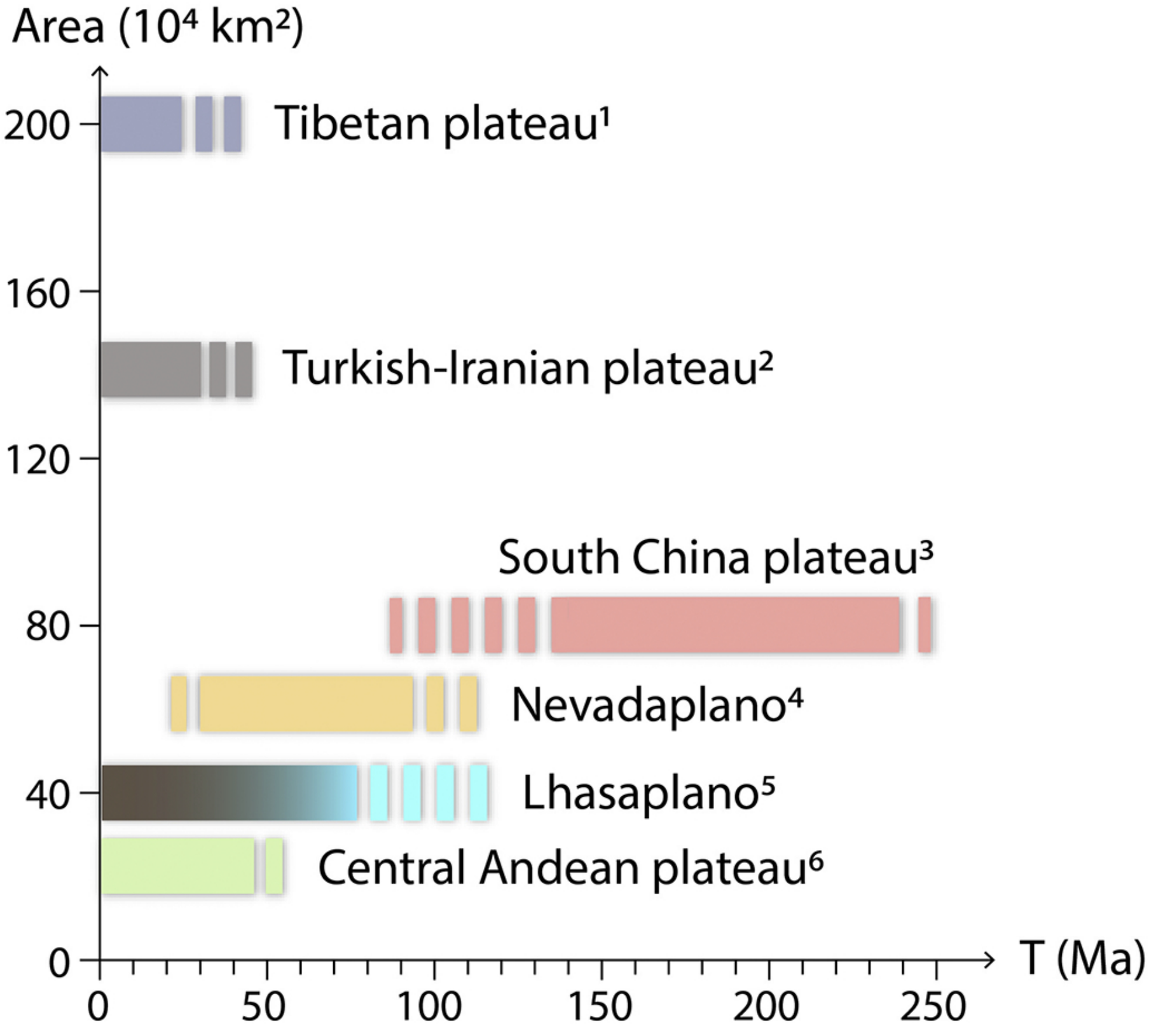
Area (10⁴ km²)
200
160
120
80
40
0
Tibetan plateau¹
Turkish-Iranian plateau²
South China plateau³
Nevadaplano⁴
Lhasaplano⁵
Central Andean plateau⁶
0
50
100
150
200
250
T (Ma)

Figure 13